Transparent polymer nanocomposites: An overview on their synthesis and advanced properties

Julien Loste, José-Marie Lopez-Cuesta, Laurent Billon, Hélène Garay, Maud Save

▶ **To cite this version:**

Julien Loste, José-Marie Lopez-Cuesta, Laurent Billon, Hélène Garay, Maud Save. Transparent polymer nanocomposites: An overview on their synthesis and advanced properties. Progress in Polymer Science, 2019, 89 (133-158), 10.1016/j.progpolymsci.2018.10.003 . hal-01934388

HAL Id: hal-01934388
https://hal.science/hal-01934388v1

Submitted on 27 Oct 2020

HAL is a multi-disciplinary open access archive for the deposit and dissemination of scientific research documents, whether they are published or not. The documents may come from teaching and research institutions in France or abroad, or from public or private research centers.

L'archive ouverte pluridisciplinaire **HAL**, est destinée au dépôt et à la diffusion de documents scientifiques de niveau recherche, publiés ou non, émanant des établissements d'enseignement et de recherche français ou étrangers, des laboratoires publics ou privés.

Contents lists available at ScienceDirect

Progress in Polymer Science

journal homepage: www.elsevier.com

Transparent polymer nanocomposites: An overview on their synthesis and advanced properties

Julien Loste[a, b], Jose-Marie Lopez-Cuesta[b], Laurent Billon[a], Hélène Garay[b, *], Maud Save[a, *]

[a] CNRS, University Pau & Pays Adour, E2S UPPA Institut des Sciences Analytiques et de Physico-Chimie pour l'Environnement et les Matériaux, IPREM, UMR5254, Hélioparc, 2 av. P. Angot, 64000, PAU, France
[b] IMT Mines Ales, C2MA, 6 avenue de Clavières, 30319 Ales Cedex, France

ARTICLE INFO

Article history:
Received 20 July 2018
Received in revised form 5 October 2018
Accepted 17 October 2018
Available online xxx

ABSTRACT

Since the last decade, there has been an increasing demand for the design of more advanced functional materials. The integration of inorganic nanoparticles to polymer matrices is a powerful tool to confer their fascinating and complementary properties to the polymer materials. Among the different polymer nanocomposites, transparent nanocomposites are of particular interest due to their significance in a wide range of applications. To achieve a high level of transparency in the nanocomposites, it is necessary to minimize the aggregation of the nanoparticles that induce significant light scattering and thus hamper the application for transparent materials. The basic concepts of light scattering, the refractive index modulation and the methods to characterize the transparency of nanocomposites are provided to introduce this review. The fabrication of the

Abbreviations: Ag, silver; Al_2O_3, alumina; APTMS, (3-Aminopropyl)trimethoxysilane; ATO, antimony-doped tin oxide; Au, gold; $CaCO_3$, calcium carbonate; CaF_2, calcium fluoride; CdS, cadmium sulfide; CdSe, cadmium selenide; CdTe, cadmium telluride; $CeFe_3$, Yb-Er; CeO_2, cerium dioxide; CTAB, cetyltrimethyl ammonium bromide; Cu, copper; DMAc, dimethyl acetamide; DMAm, *N,N*-dimethylacrylamide; DMF, *N,N*-dimethylformamide; DMSO, dimethyl sulfoxide; DVB, divinylbenzene; EPDM, ethylene propylene diene monomer rubber; Fe, iron; Fe_2O_3, ferric oxide; FeS_2, iron disulfide; GdOF:Ce, gadolinium oxyfluoride doped cerium; Ge, germanium; ITO, tin-doped indium oxide; LDPE, low density polyethylene; LLDPE, linear low density polyethylene; MAPTMS, 3-methacryloxypropyltrimethoxysilane; $MnZnFe_2O_4$, manganese-zinc ferrite; P(S-co-AN), styrene-acrylonitrile copolymer; P(S-co-MAh), styrene-maleic anhydride copolymer; P2VP, poly(2-vinylpyridine); PA, polyamide; PBMA, poly(butyl methacrylate); PBMA, poly(butyl methacrylate); PbS, lead sulfide; PbUa, poly(butyl acrylate); PC, polycarbonate; PDAM, poly(diallyl maleate); PDMAm, poly(*N, N*-dimethylacrylamide); PDMS, polydimethylsiloxane; PE, polyethylene; PEG, polyethylene glycol; PES, polyether Sulfone; PET, polyethylene Terephthalate; PEVA, EVA, poly(ethyl vinyl acetate); PGMA, poly(glycidyl methacrylate); PHEMA, poly(hydroxyethyl methacrylate); PI, polyimide; PITE, polyimidoether; PMMA, poly(methylmethacrylate); PNVP, poly(*N*-vinyl 2-pyrrolidone); Pox, poly(2-oxazoline); PS, polystyrene; PSAN, polystyrene acrylonitrile; PSS, polystyrene sulfonate; PTU, polythiourethane; PU, polyurethanee; PUA, polyurea; PUMM, poly(urethane-méthacrylate); PVA, PVAc, poly(vinyl alcohol), polyvinyl acetate; PVB, polyvinyl butyryl; PVC, polyvinyl chloride; PVD, polyvinylidene chloride; PVP, poly(vinylpyrrolidone); S, sulfur; SiO_2, silica; Ta_2O_5, tantalum pentoxide; Tb, terbium; TEOS, etraethoxysilane; THF, tetrahydrofuran; TiO_2, titanium dioxide; TMOS, tetramethoxysilane; TMSPMA, (Trimethoxysilyl)propyl methacrylate; UEA, urethane epoxy acrylate; YAG:Ce3+, yttrium aluminium garnet doped cerium; Yb3+:CaF_2, trivalent ytterbium doped calcium fluoride; ZnO, zinc oxide; ZnS, zinc Sulfide; ZrO_2, zirconium dioxide

* Corresponding authors.
Email addresses: Helene.Garay@mines-ales.fr (H. Garay); maud.save@univ-pau.fr (M. Save)

https://doi.org/10.1016/j.progpolymsci.2018.10.003
0079-6700/ © 2018.

UNCORRECTED PROOF

Keywords:
Polymer nanocomposite
Transparency
Polymer hybrid
Nanoparticles
Grafting
Optical properties

transparent nanocomposites has been the subject of many efforts to develop methods to limit aggregation. To address this challenge, several methods have been implemented to control the polymerization process, the nanoparticle synthesis, and the polymer-nanoparticle interface together with the polymer casting or processing. The main methodologies developed to fabricate transparent nanocomposites are discussed according to four main categories: the blending of nanoparticles and polymer; the *in-situ* polymerization in the presence of pre-formed nanoparticles; the *in-situ* nanoparticle synthesis in a pre-formed polymer matrix; and finally the simultaneous polymerization and *in-situ* nanoparticle synthesis. The few studies dealing with casting of polymer solution loaded with core-shell nanoparticles are also discussed. In light of the literature on polymer nanocomposites, this review focuses on transparent nanocomposites with special attention given to the level of transparency and how this transparency is assessed for each study claiming transparency of the nanocomposite. For each class of nanocomposites, it is of great importance to provide an overview of the different level of transparency according to the thickness of the polymer material. The second part of the review provides a thorough overview of the properties investigated in transparent nanocomposites with attention paid to the characterization of transparency. The transparent nanocomposites were described according to the targeted properties which are primarily the improvement of mechanical properties, thermal stability, barrier properties, magnetic properties and the optical properties. The optical properties have been the most thoroughly investigated due to the myriad inorganic nanoparticles exhibiting an excellent wide range of optical properties. Thus, the present review also describes the polymer/nanoparticle systems designed for the fabrication of transparent polymer nanocomposites with advanced optical properties: UV or IR-filtering properties, photoluminescence, ability to produce extreme refractive index, dichroism or non-linear optical properties.

© 2018.

1. Introduction

Polymers are widely used for their relatively low production cost, light weight and ease of processing. Considerable progress has been made over the preceding decade in the development of high-performance polymers. Due to their structure, and to the ionic character of their bonds, inorganic materials lead to physical properties such as magnetism, conductivity and phonon absorption. Nevertheless, the expensive cost of their manufacture, and the difficulty to shape and process them limit their use [1,2]. The incorporation of inorganic particles into a polymer matrix takes advantage of both components to create original composite materials with new properties. These particles were first available in micrometer sizes, but size reduction to the nanometer scale has allowed new properties for the composites to be achieved due to the huge increase of specific area of the particles. The most commonly used polymer matrices include amorphous thermoplastics (e.g., poly(methyl methacrylate) (PMMA), polycarbonate (PC), polystyrene (PS)) and thermosets (e.g., epoxy, silicone). Different kinds of inorganic fillers are currently incorporated in those matrices, in particular oxides (e.g., SiO2, TiO2, CeO2, ZnO, ITO, ATO, ferric oxide), semiconductors (e.g., CdS, PbS, CdTe, CdSe), minerals (e.g., clays, CaCO3), metal and metal alloys (e.g., Au, Ag, Cu, Ge, Fe) [2]. Many reviews on nanocomposites materials have been reported in the literature, with different objectives. Although some raise the problem of optical transparency [1–15], to our best knowledge, none have focused on the nanocomposite transparency, with the aim of comparison of the performances achieved. The incorporation of inorganic particles into a polymer matrix often induces modifications of the perceived visual appearance of the composite, including the loss of transparency. This loss of transparency can be reduced by using nanoparticles with dimensions much smaller than the wavelength of the light to minimize scattering phenomenon. However, incorporating nanoparticles in a polymer without any aggregation is a challenge. The intrinsic properties may be degraded because of the aggregation state of the nanoparticles or due to poor affinity with the matrix. This review focuses on transparent nanocomposites with inorganic particles and organic polymer matrices. The key parameters to retain transparency will be defined and reviewed. The scattering of light by particles is well known. The theory of Mie [16] for light scattering from spherical particles large compared with the wavelength of light, and the simpler theory of Rayleigh [17] for smaller particles give the key parameters to minimize the scattering: size of the particles, and difference between the refractive index of the particles and of the polymer matrix.

To minimize the light scattering, the selection of nanometric particles is necessary as micrometric particles scatter light more intensively and in the same way for each wavelength of the visible light, giving a "milky" aspect to the composite. In most of the articles cited in this review, the transparency of the composite is assessed through transmission of visible light. Different experimental parameters like the thickness of the nanocomposite, the nanoparticle content or the chemical nature of the polymer and nanoparticles can affect this level of transparency. To provide a critical review on the transparency of nanocomposites, the different types of nanocomposites are classified in several tables that report in detail for each nanocomposite the type of polymer matrix, the nature of the nanoparticles, the content of nanoparticles and the thickness of the nanocomposite used for transparency measurement together with the appreciation of the level of transparency.

This literature review is divided into five parts. In the first part, we will present the fundamental phenomena of interactions between light and matter. In the second, the different concepts developed to favor transparency of nanocomposites and particularly the refractive index matching will be discussed. The third section focuses on the way to characterize such transparency. The fourth part of the review examines different methodologies implemented to fabricate the nanocomposites with the attempt to reach transparent materials. Finally, the fifth section focuses on the targeted properties and applications regarding the intrinsic properties of the nanoparticles with special attention to the quality of nanocomposite transparency. The values of transmittance will be outlined and compared, whereas the readers interested in the targeted properties are invited to refer to the original articles.

2. Theory of light scattering by particles

The transparency of a composite can be outlined as the physical property of permitting the light transmission through the composite. In composites, when fillers are incorporated into a transparent matrix a loss of transparency can be observed and leads to opaque composites. In fact, the matrix can be considered as a non-absorbing uniform medium in which the light passes through without deflection. By adding fillers with a different refractive index, the light interferes with the particles. The main phenomena occurring are scattering and

UNCORRECTED PROOF

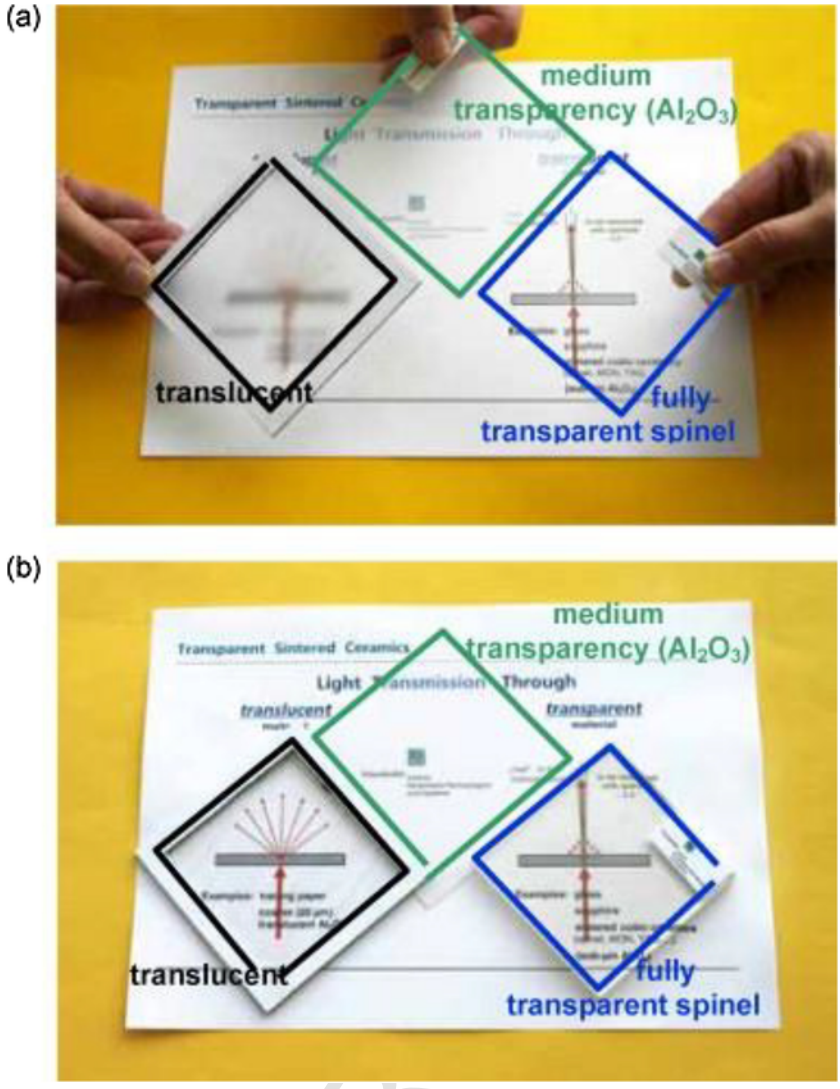

Fig. 1. Comparisons showing the importance of the relative position between the sample film above an image in estimating the transparency of a film; the image appearance may reveal differing optical properties if the film is far enough away from the image, as in Part A, but the distinctions may be suppressed if the film-image separation is decreased, as in Part B. [50], Copyright 2008. Reproduced with permission from Elsevier Ltd.

absorption of light by the particles. In this section, as we are interested in transparent composites in the visible domain, we will only focus on non-absorbing particles for wavelength in the range of 400 nm $< \lambda <$ 800 nm. So, in our case, the loss of transparency in the visible domain is attributed to the scattering of light by particles. Scattering of light by particles is closely linked to particle dimensions and the difference of refractive index between particles and the medium. The phenomenon may be explained by different theories depending on the size of particles. The Mie theory [16], established in 1908, describes the scattering of a harmonic electromagnetic plane wave by a spherical, homogeneous and isotropic particle located in a non-absorbing medium. It rigorously solves the Maxwell and Wave Equations in spherical coordinates by the separation of variables method for appropriate boundary conditions. This theory is only exact when considering isolated particles, i.e.,the light scattered by a particle will not be scattered again by other particles, so there is no multiple scattering. This condition applies with a mutual distance between particles of approximately three times the radius of particles [17]. For nanocomposites, we assume that the condition applies with low particle concentration, of the order of some percent. In this review, the mathematical resolution has not been detailed. The resolution can be followed in its entirety step by step in the complete books of Bohren and Huffman [18], Van de Hulst [17], Kerker [19] and Stratton [20]. If the dimension of the particle is small compared to the wavelength ($D/\lambda << 1$, with D the particle diameter), the light scattering by particle is then described by the Rayleigh theory. The Rayleigh theory is an asymptotic special case of the Mie theory. The intensity of scattered light by a particle for an un-polarized incident radiation is now given by the equation

$$I = \frac{8\pi^4 a^6}{r^2 \lambda^4} \left(\frac{n^2 - 1}{n^2 + 2} \right)^2 \left(1 + cos^2\theta\right) I_0 \quad (1)$$

Where $n = n_1/n_2$ is the refractive index of the particle divided by the refractive index of the medium, a is the radius of the particle, λ is the wavelength, θ is the angle between the incident ray and the observa-

UNCORRECTED PROOF

Table 1
Particle dispersion in the monomer followed by in-situ polymerization.

Polymer	*Nanoparticles*	*Initiator*	*Reference*
Poly(urethane methacrylate)	ZnS	Darocur 1173, AIBN	[99]
PS	CdTe nanocrystals	AIBN	[100]
PHEMA	ZnO modified TMSPMA	AIBN	[101]
PMMA	ZnO	AIBN, BPO	[102]
PMMA	ZrO_2	AIBN	[91,92]
PMMA	TiO_2	AIBN	[105]
PMMA	Iron Oxide	AIBN	[106]
PMMA	CaCO3	DPO	[107]
PMMA	Methacrylate/CTAB -treated Laponite clay	AIBN	[108]
PMMA	[11-(2-bromo-2-ethyl)propionyloxy] undecylchlorodimethylsilane] -grafted Laponite clay	Grafted ATRP initiator	[108]
PMMA	TiO2 treated modified with 6-palmitate ascorbic acid	AIBN	[105]
PMMA	GdOF:Ce, Tb nanoparticles	AIBN	[109]
PBMA	ZnO	AIBN	[110]
PC	Aluminum oxide nanowhiskers (D = 2 - 4 nm, L = 2800 nm)	BPA + TEA + Pyridine + Triphosgene	[111]
Crosslinked matrix (S, DVB, DMAm)	ZnS	AIBN	[112]
Poly(4-vinyl benzyl alcohol) or resin of ethoxylated (6) bisphenol A dimethacrylate	Anatase TiO2 surface-modified by carboxylic acids (acetic, hexanoic or phenyl acis)	Irgacure 651 photoinitiator	[86]
Poly(urethane acrylate)	TMSPMA modified ITO NPs	Irgacure (1173, 184) photoinitiator	[87]
Polyhydroxydiethoxylate bisphenol-A dimethacrylate and methacrylic acid ester dodecyl methacrylate	CaF_2	Benzoyl peroxide	[113]
Epoxy-acrylate resins	ZnO@ APTMS	Thermal or UV-curing	[93]
Epoxy resin	SiO2@TiO2	Thermal curing	[30]
Epoxy resin	ZnO@SiO2	Thermal curing	[30]
Epoxy resin	ZrO2	Thermal Curing	[89]
Epoxy resin	Bentonite Clay@PGMA	Thermal Curing	[95]
Silicone resin	Colloidal mesoporous SiO2	Curing	[94]
PDMS	Ag nanowires	Thermal curing	[114]

tion direction, and r is the distance between the particle center and the observer.

The Rayleigh theory has been used for describing the reduction of light intensity due to scattering in composites. To our knowledge two expressions, proposed by Novak [8] (Eq. (2)) and Nussbaumer [21] (Eq. (3)), can be found in the transparent composites literature.

$$\frac{I}{I_0} = e^{-\left[\frac{3V_p x r^3}{4\lambda^4}\left(\frac{n_p}{n_m}-1\right)\right]} \quad (2)$$

Where r and n_p are the radius and the refractive index of a spherical particle, respectively, n_m is the matrix refractive index, V_p is the volume fraction of the particles, x is the optical path length, I is the intensity of the transmitted light by the composite and I_0 is the intensity of the incident light.

$$\frac{I}{I_0} = e^{-\left[\frac{32V_p x \pi^4 r^3 n_m^4}{\lambda^4}\left|\frac{\left(\frac{n_p}{n_m}\right)^2-1}{\left(\frac{n_p}{n_m}\right)^2+2}\right|^2\right]} \quad (3)$$

The equation proposed by Novak cannot be applied if n_m is greater than n_p (for example silica n = 1.4631 embedded in a matrix of PMMA n = 1.4893). In this case I would be above I_0, which is physically incorrect. For both equations if $n_p = n_m$ (called refractive index matching) the scattering tends to be zero and the transmission $T = \frac{I}{I_0}$ is equal to 1 (i.e. the composite is totally transparent).

3. Refractive index matching

The scattering of visible light in composites can be strongly decreased by using nanoparticles in comparison to micro-size particles. However, even with small particles, for most of the inorganic/organic systems the consistent difference of refractive index leads to significant light scattering and to a loss of transparency in composites. As shown before in equations (and E3) given by Novak and Nussbaumer, the intensity of scattered light by particles in composites can be suppressed if the refractive indices of matrix and particles are matched ($n_p = n_m$).

Following this reasoning, several studies have been conducted to obtain transparent composites by carefully selecting combinations of inorganic/organic materials having the same refractive index or the closest possible. Lin et al. [22] employed refractive index matching to obtain highly transparent composites of PMMA reinforced with glass fibers. The matrix and fillers had a temperature-dependent refractive index difference of only 6.3×10^{-4} at the best case temperature of 31.5 °C, and composites 0.68 mm thick with 10.4 vol% of glass fibers with an overall transmission of 92% at that temperature. In a similar approach, Yu et al. [23] demonstrated completely transparent composites of PMMA filled with polyvinyl butyral nanofibers with perfectly matched refractive indices of matrix and filler. Gilmer et al. [24] studied the transparency of semi-interpenetrating polymer networks composed of PMMA and aromatic/aliphatic siloxane. They compared the transmittance of 1 mm thick films of various compositions and found that PMMA films had a transmittance of 92% when aromatic siloxane (polydiphenyl siloxane) was added. The transmittance was 79% and for PMMA/aliphatic siloxane films the transmittance dropped to 0%. Refractive indices of PMMA, aromatic siloxane, and aliphatic siloxane were 1.49, 1.49 and 1.43, respectively; for

UNCORRECTED PROOF

Table 2
In-situ particle synthesis in pre-formed polymer matrix.

Polymer	Nanoparticle	Particle synthesis process	Referen
PMMA	SiO_2	Sol-gel	[102,103
PVA	SiO_2	Sol-gel	[104,105
PVAc	SiO_2	Sol-gel	[102,106
POx	SiO_2	Sol-gel	[107,134
PEVA	ZnO, TiO2	Sol-gel	[146]
PNVP	SiO_2	Sol-gel	[102,134
PDAM	SiO_2	Sol-gel	[102,134
PA-6,6	SiO_2	Sol-gel	[122]
Cellulose acetate	SiO_2	Sol-gel	[123]
Modified chitosan	SiO_2	Sol-gel	[124]
PDMS	SiO_2, TiO_2	Sol-gel	[125]
PES	SiO_2	Sol-gel	[126]
PS	SiO_2	Sol-gel	[134]
P(S-co-TMSPMA)	SiO_2	Sol-gel	[136]
P(MMA-co-TMSPMA)	SiO_2/ZnO, TiO_2	Sol-gel	[120,122
Modified polyphosphazene	SiO_2, TiO_2	Sol-gel	[121,115
PS	Phenyl- SiO_2	Sol-gel	[130]
PSS	Aminopropyl-SiO_2	Sol-gel	[129]
Polyimide	Phenyl- SiO_2	Sol-gel	[131]
PSAN	TiO_2	Sol-gel	[133]
P(S-co-MAh)	TiO_2	Sol-gel	[138]
Poly(amide-imide)	TiO_2	Sol-gel	[137]
Poly(N-vinyl pyrrolidone)	ZnO	Sol-gel	[140]
Crosslinked PSS	γ-Fe2O3	Metallic ion reduction	[141]
PVA	Gold, silver	Metallic ion reduction	
Poly(2-methoxy-5-(2′-ethyl-hexyloxy)-p-phenylene vinylene, PE, PB, PD, PS	PbS nanocrystals	Lead and Sulfur precursors in polymer solution	[144]
PVP, PVA	Nanocrystalline iron disulfide (FeS2)	FeCl3 + CH_4N_2S, autoclave 150 °C	[145]
Sulfonated PS	CdS nanoparticle	Cadmium acetate + thioacetamide	[147]
PVA	CdS nanoparticle	Cd(II) bis(N-ethyl-N-phenyl dithiocarbamate) precursor + high intensity laser	[143]

composites with mismatched refractive indices, the transmittance sharply decreased. Comparable investigations were conducted by Tan et al. [25] by studying nanocomposites of unmodified CeF_3: Yb-Er in PMMA or PS matrix. PS nanocomposites exhibited better transparency compared to PMMA nanocomposites. In the case of the PS matrix, the refractive index matching conditions were fulfilled, whereas in the case of PMMA matrix, refractive index mismatch affected the transparency. This tendency increased with the increase of particle loading.

Unfortunately, only a few combinations of inorganic fillers and polymer matrix have almost equivalent refractive indices. When refractive indices are not naturally equivalent, the use of core@shell particles is a promising strategy to match the refractive index of the particle to that of the matrix. A third material with a refractive index greater than (or less than) that of the matrix is used to form a shell around the inorganic core which has a refractive index less than (greater than) the matrix. For a given shell thickness, the average refractive index of the core@shell particle matches that of the matrix promoting suitable conditions for transparency of the composite. The core@shell particle can be considered as a homogeneous particle with a constant refractive index only if the particle is very small compared to the wavelength ($D/\lambda<<1$). The refractive index of the core@shell particle depends on the optical properties and volume fractions of both core and shell constituents [26]. The value of the refractive index of a core@shell particle may be estimated theoretically be by different effective medium models. Considering core@shell particles as discrete inclusions in a homogeneous medium and for particles with very small dimension compared to the wavelength, the Maxwell-Garnett theory [27,28] is considered to be appropriate. The effective dielectric constant of a core@shell particle is given by equation Eq. (4):

$$\varepsilon_{eff} = \varepsilon_{shell}\left(1 + 3\frac{\varphi x}{1-\varphi x}\right) \tag{4}$$

$$x = \frac{\frac{1}{3}\left(\varepsilon_{core} - \varepsilon_{shell}\right)}{\varepsilon_{core} - \frac{1}{3}\left(\varepsilon_{core} - \varepsilon_{shell}\right)} \tag{5}$$

$$\varphi = \frac{V_{core}}{V_{core} + V_{shell}} \tag{6}$$

With ε_{eff} ε_{core} and ε_{shell} the dielectric constant of the core@shell, the core particle and the shell, respectively, and φ the ratio of the volumes V_{core} and V_{shell} of the core and the shell, respectively. The dielectric constant is related to the refractive index by $\varepsilon = n^2$.

The Maxwell-Garnett theory is an effective medium model for composites with low filler concentrations (the order of some wt%). For higher loaded composites, other effective medium theories, such as the Bruggeman model are more appropriate [26,29].

Various core@shell particles have been synthesized and dispersed in different polymeric matrices to obtain transparent composites. This

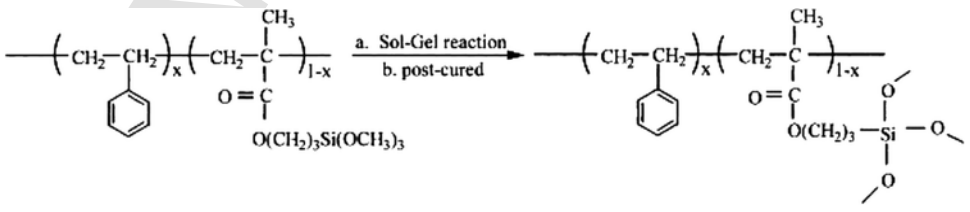

Fig. 2. Fabrication of transparent nanocomposites synthesized via sol-gel process from a trimethoxysilyl-based polystyrene copolymer. [136], Copyright 2000. Reproduced with permission from Elsevier Ltd.

UNCORRECTED PROOF

Table 3
Simultaneous particle and polymer matrix synthesis.

Polymer	Nanoparticle	Methods of polymerization / particle synthesis	Reference
PHEMA	Silica	Radical polymerization / Sol-gel reaction	[139,140]
Poly(alkyl acrylate)	Silica	Radical (photo)polymerization / Sol-gel reaction	[141,144]
PMMA	Silica	Radical polymerization / Sol-gel in inverse microemulsion	[156]
Poly(Cyclic alkenyl)	Silica	Ring opening polymerization / Sol-gel reaction	[123]
Aromatic polyamide	Silica	Step-growth polymerization / Sol-gel reaction	[151]
Epoxy resin	Silica	Step-growth polymerization / Sol-gel reaction	[152]
P(MMA-co-TMSPMA)	Titanium dioxide	Radical polymerization / Sol-gel	[155]
PMMA	Cadmium Sulfide	Radical polymerization / Reaction Cd^{2+} and S^{2-} in inverse microemulsion	[157]
PMMA	Palladium, Platinium, Silver, Gold	Radical polymerization / metallic ion reduction	[138,151]
Crosslinked Poly(tetrahydrofurfuryl methacrylate)	Bismuth	Radical polymerization / reduction	[159]
PMMA	ZnO nanocrystals	Radical polymerization / in-situ thermal decomposition	[161]
PMMA	ZnO	Radical polymerization of MMA / Sol-gel reaction	[102]

Table 4
Dispersion of pre-formed core@shell nanoparticles in a polymer solution followed by solvent evaporation to form transparent nanocomposites.

Polymer	Core − Shell Nanoparticles	Reference
PS	CeO2@SiO2	[162]
PVA	SiO2@Ag	[163]
PS	CeO2@MAPTMS	[78]
P(S-co-MAh) copolymer	Alumina@APTMS	[55]
PMMA, PI, PS, P2VP	(Ag, CdSe, PbS, Au, Fe_2O_3, ZnO)-grafted with polymer brushes	[164]
PS	CeO2@PMMA	[37]
Epoxy matrix	TiO2@PGMA	[165]
P(S-co-AN) copolymer	SiO2@ P(S-co-AN)	[60]

review is focused on core@shell particles with an inorganic core, starting with inorganic core@shell particles made of both inorganic core and inorganic shell. For example, Li et al. [30] synthesized transparent composites made of epoxy matrix filled with silica@titania core@shell particles. The transmittance of composites was measured for different shell mass compositions ranging from 0 to 60 wt%. Highly transparent composites were achieved for a shell content of 36.5 wt%, i.e., when the composite composition was the closest of the ideal composition completing the refractive index matching. In this study, the theoretical core@shell refractive index was estimated by taking the average value of components refractive indices, estimated by formula (Eq 7):

$$n^2_{core@shell} = \sum_i n_i^2 V_i \quad (7)$$

Where n_i and V_i are the refractive index and volume fraction of individual components, respectively. The same strategy was also used to incorporate Al_2O_3@SiO_2 in a PC matrix [31], SiO_2@TiO_2 in dental resin [32], ZnO@SiO_2 in epoxy [33] and silicone matrix [34], the combination of SiO_2/Ta_2O_5 [35] and SiO_2/Ytterbium [36] in acrylic matrix. In all these examples, composites exhibited the highest transparency when core@shell particles were synthesized in a composition as close as possible to the perfect composition satisfying the refractive index matching conditions. Full inorganic core@shell particles showed some dispersion limits in polymer matrix since inorganic particles have a strong tendency to aggregate. This can lead to a deterioration of the composite transparency and overall properties.

Covering the inorganic core with a polymer shell offers an interesting option to enhance the dispersion of core@shell inside the polymer matrix and to avoid particle aggregation. Many studies reported the grafting of polymer chains onto inorganic particles to design core@shell particles based on an inorganic core and a polymer shell. Two studies reported the refractive index matching strategy to fabricate transparent nanocomposite with inorganic/polymer core@shell particles. Bombalski et al. [26] synthesized SiO_2@PS core@shell nanoparticles, using a grafting from technique to graft PS chains onto a silica surface. The length of the PS chains (subsequently the thickness of the polymer shell) was controlled by using an Atom-Transfer Radical Polymerization. SiO_2@PS nanoparticles were dispersed in toluene and the Maxwell-Garnett theory was employed to determine that an ideal particle mass composition of m(PS)/m(SiO_2) ≈ 0.19 matched the refractive index of toluene. Experimentally, the transparency of particles in toluene was investigated as a function of mass composition m(PS)/m(SiO2) (0.12, 0.22, 2.5 and 7.5). The most transparent system was obtained for a mass composition of 0.22, the closest to the theoretical refractive index matching conditions (0.19). The authors claimed that those results obtained in a liquid embedding medium will be analogous in a polymer matrix. More recently, Parlak and Demir [37] confirmed this conclusion with composites composed of CeO_2@PMMA nanoparticles in PS matrix. The surface of ceria particles was modified with PMMA chains by coupling a grafting through technique and free radical polymerization. Unmodified ceria in PS resulted in opaque composites. However, the transparency of the composite was notably enhanced with CeO_2@PMMA particles, especially for PMMA with shell thickness of 9 nm. The theoretically perfect shell thickness was estimated by the Maxwell-Garnett theory to be 7 nm. The authors tried to adjust the shell thickness to 7 nm but they did not manage to synthesize PMMA layer thinner than 9 nm.

Recently, an inverse approach of the refractive index matching was developed. The structure of the matrix was modified to tune the matrix refractive index to that of the particles. All investigations listed below were performed to match the refractive index of the matrix with that of glass fibers. Matsukawa et al. [38] tuned the refractive index of a resin matrix by varying the composition of photo-cured mixture obtained by thiol-ene chemistry with poly(thiopropylsilsesquioxane) and allyl compounds. Krug et al. [39] tailored the refractive index of epoxy-glass fibers nanocomposite via the addition of octakis[[3-(2,3-epoxypropoxy)propyl] dimethylsiloxy] silsesquioxane. Shin et al. [40] synthesized a resin matrix with photocurable isosorbide dimethacrylate and cardo-type fluorene acrylate. In each case, highly transparent composites were obtained when the matrix refractive index matched that of the glass fibers. This new approach

UNCORRECTED PROOF

Table 5
Summary of transparent nanocomposites studied for their mechanical properties. NPc is the nanoparticle content.

Polymer matrix	Nanoparticles	Transparency	Film thickness	NPs Content (wt.%)	ref
PC	Coated Al_2O_3	T(λ, NPc) from 5 to 60 % UV-Vis + photos	2 mm	1 to 2	[56]
	SiO_2	Just announced	/	/	[60]
	Al_2O_3	T(λ) from 50 to 80 % UV-Vis	0.15 mm	2	[111]
PET	TiO_2	T(λ, NPc) from 5 to 40 % UV-Vis	80 µm	1 to 5	
PLA		T(λ, NPc) from 5 to 17 % UV-VIs	80 µm	1 to 5	
PVC	bentonite	Just photos	3.25 mm	5	[69]
LLDPE	clay	Just announced	/	Up to 10	[73]
LDPE	starch	T(λ) from 30 to 55 % Uv-Vis	/	20	[74]
PMMA	clay	T(λ, NPc) from 78 to 90 % UV-Vis + photos	100 µm	1 to 5	[76]
	ZrO_2	T(λ, NPc) from 65 to 85 % UV-Vis	/	Up to 15	[103]
		T(λ, NPc) from 70 to 85 % UV-Vis + photos	1 mm	Up to 7	[104]
	ZnS	T(λ, NPc) from 25 to 90 % UV-Vis + photos	4 mm	5 to 15	[112]
	SiO_2	T(λ, NPc) from 30 to 90 % UV-Vis	about 1 mm	4 to 8	[177]
PMMA	TEOS	Visual appreciation	/	/	[115]
PVP					
PDMAm					
PVA					
PS	ZnO	Just announced	/	/	[81]
	PS grafted SiO2	Just announced	/	/	[[180]]
	PS grafted TiO2	T(λ, NPc) from 20 to 70 % (UV-Vis)	70 µm	Up to 1.05	[178]
PBMA	ZnO	T>90 % UV-vis + photos	100 µm	5	[110]
Epoxy resin	ZrO_2	T(λ, NPc) from 10 to 80 % (UV-Vis + photos)	4 mm	2 to 16	[89]
	Organo-modified bentonite clay	photo	3 mm	3	[95]
UEA	SiO_2	T(λ, NPc) from 80 to 90 % (UV-Vis)	10 to 30 µm	5, 10 and 15	[176]
PVA	SiO_2	Just announced	50 µm	20 and 33	[118]
	clays	T(λ, NPc, type of clay) from 10 to 80 % UV-Vis + photos	25 µm	Up to 68	
PA	SiO_2	T(λ, NPc) from 40 to 70 % UV-Vis	100-150 µm	Up to 5	[122]
		T(λ, NPc) from 78 to 87 % UV-Vis	120 µm	Up to 20	[174]
PDMS	Silica colloidal crystal	>90 % (UV-Vis + photos) but less under stress	1.25 cm	Layer of SCC	[[181]]
Poly [bis(methoxyethoxyethoxy)-phosphazene]	TEOS	Just announced	/	23	
Polyimide	SiO_2	Just announced	/	45	[131]
Poly(amide-imide)	TiO_2	Visual appreciation	15-70 µm	3.7 to 17.9	[137]
Silicone	SiO_2	T(λ) = 40 to 60	50 µm	15	[94]
Epoxy resin		Just photos - poor transparency	50 µm	20	
PU	ZnO	Just announced		Up to 2	[173]
Poly(urethane dimethacrylate)	Montmorillonite	T(λ, NPc) from 50 to 90 %	100 µm	1, 3 and 5	[179]
Fluorinated polyimide	2D fluoro-graphene	T>90%	3 µm	0.25 to 1	[182]

appeared to be efficient for transparent composites filled with glass fibers ($n \approx 1.5$). Nevertheless, this strategy seems hardly feasible for inorganic fillers with higher refractive indices ($n > 2$). In such composites, the choice of matrix components to obtain high refractive index is rather limited. Few studies focused on the temperature dependent matching/mismatching refractive indices of transparent composites. Because the refractive index of a material is temperature-dependent while the matrix and fillers have different thermo-optic coefficients, transparent composites fulfilling the refractive index matching conditions at room temperature turn into opaque composites when increasing the temperature. This phenomenon was reported by Lin et al. [22] for a composite made of PMMA filled with glass fibers mentioned in the preceding, with a maximum transparency at 31.5 °C. Cheng and Hozumi [41] showed similar behavior with silica particles in a silicone matrix. The composite exhibited reversible thermo-responsive transparency properties, with a critical temperature of 80 °C to shift the refractive indices from matching to mismatching and so to turn a transparent composite into an opaque composite. Brien et al. [42] attempted to minimize the temperature-dependent refractive index mismatching for glass-polymer composite. To improve the temperature-dependent performance of the transparent composite, they created a polymer-nanoparticle interphase between the matrix and glass fibers by coating conventional micron-sized glass fibers with a mix of polymer and glass nanoparticles. At temperatures higher than the refractive index matching temperature, the nanoparticle interphase has an intermediate refractive index between those of matrix and glass fibers.

4. Characterization of composite transparency

The physical property of transparency is mainly based on the measurement of transmittance of visible light through the material. The comparison of the transparency of different composites reported in the literature is a delicate issue and is difficult to accurately report. The transmittance of the composite depends on many factors, which are either related to the intrinsic material properties such as the particle size and the refractive index of the components, or to the composite fabrication such as the composite thickness, the surface roughness, the filler concentration and dispersion state of particles. This multitude of parameters, which vary from one study to another, partially misrepresents the comparison. The transparency of a composite can be defined as the perceptual property corresponding to the physical

UNCORRECTED PROOF

Table 6
Transparent nanocomposites with thermal stability properties. NPc is the NPs content.

Polymer matrix	Nanoparticles	Transparency	Thickness	NPs Content (wt.%)	ref
PMMA	SiO_2/ZrO_2	T(λ, NPc) from 90 to 97 % UV-Vis + photos	/	Up to 20	[135]
	clay	Just announced	/	/	[68]
		T(λ, NPc) from 78 to 90 % UV-Vis + photos	100 µm	1 to 5	[76]
		T(λ, NPc) from 10 to 68 % UV-Vis + photos	3 mm	0.39 to 4.60	[183]
	ZrO_2	T(λ, NPc) from 70 to 85 % UV-Vis + photos	1 mm	Up to 7	[104]
	CdS	Abs UV-Vis only	/	/	[184]
	ZnO	Abs UV-Vis + photos only	45 µm	8	[161]
		T(550 nm) = 91 %	2 µm	Up to 11	[185]
	TiO_2	Just announced	/	/	[61]
	ZnS	T(λ, NPc) from 25 to 90 % UV-Vis + photos	4 mm	5 to 15	[112]
PS	ZnO	Just announced			[81]
PVA	TiO_2	T(λ, NPc) from 5 to 80 % UV-Vis	100 to 200 µm	5 to 20	[79]
	$Mg(OH)_2$	T(λ, NPc) = 86 to 98 %	500 µm	10 to 50 phr	[186]
PA	SiO_2	T(λ, NPc) from 40 to 70 % UV-Vis	100-150 µm	Up to 5	[122]
PnBA	ZnO	T = 90%	100 µm	5 and 60	[110]
Polyimide	SiO_2	Just announced		45	[131]
	Montmorillonite or synthetic mica	Just announced	20 µm	1,2 and 4	[77]
Polyepoxy	ZnO	T> 90%	2 -2.5 µm	7 to 13	[187]
Poly(acrylate)	SiO_2	photos	1 mm	Up to 3	[188]
PEVA	CdS-ZnS QDs @ SiO_2	T(L, d-core) : 50 to 80 %	500 µm	1%	[189]

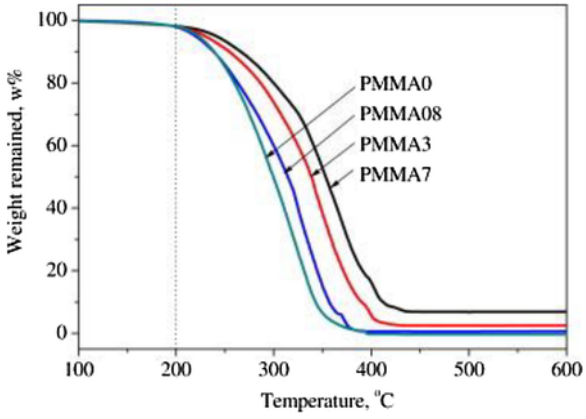

Fig. 3. TGA curves of a PMMA matrix filled with 0, 0.8, 3 and 7 wt% of zirconia nanoparticles. [104], Copyright 2011. Reproduced with permission from Elsevier Ltd.

phenomenon of permitting light transmission through the composite [43]. Considering this definition, a composite can be described by different states of transparency. A fully transparent composite transmits all the light with no diffusion. On the contrary, an opaque composite does not transmit the light at all and no object may be seen through it. The term translucent composite includes all the intermediate states of transparency, when the light is diffusely transmitted and the object beyond the composite may be seen through it, but not clearly [44]. How a composite is seen and its perceived appearance is a possible method of qualitatively evaluating composite transparency. A transparent composite can be defined by its physical transmittance but when transparency is strategic, going further by measuring the perceptual or psychophysical transparency can be useful for integrating the human perception. The challenge in transparency characterization is finding parameters of instrumental characterization that account for the perceived appearance in addition to the physical transmittance parameters. The perception of transparency by human eyes requires the use of sensory analysis.

In most publications dedicated to transparent composites, the transmitted light is partially measured. Generally, only the specular or direct transmission is measured with a spectrophotometer. For this measurement, the analyzed composite is illuminated at a normal incidence by a light source of controlled intensity and the direct transmitted light is collected by a detector located in the incident direction. The transmission is characterized at all wavelengths of visible domain but sometimes only the wavelength at 550 nm is selected, where the human eye has the highest sensitivity [37]. The regular transmittance is given by Eq. (8):

Table 7
Transparent nanocomposites with barrier properties. NPc is the NPs content.

Polymer matrix	Nanoparticles	Transparency	Thickness	NPs content wt.%	ref
LLDPE	2 Clays	T(660 nm) = 50 -68 %	55-60 µm	33	[72]
	Clay	Just announced	/	Up to 10	[73]
Polyethylnimine	Clay	T(pH) = 93 to 97 %	60 nm	84.3	[190]
Xanthan-Starch	Clay	TNPc) = 50-57 %	/	2.5-5	[71]
PVA	Clay	T(λ, NPc, type of clay) from 70 to 97 % UV-Vis + photos	25 µm	Up to 68	[196]
PMMA	Ag	Just Announced	/	/	[160]
Chitosan/PEG/Calcium silicate	ZnO	T = 60% (UV-Vis)	/	11 mol. %	[191]
Epoxy	α-ZrP	Just photos	25 µm	10	[194]
		T(λ) from 80 to 90 %	1-2 µm	5	[195]
	SiO_2	T = 90%	50 µm	Up to 30	[193]
Sulfonated poly(arylene ether sulfone)	TiO_2 / ZrO_2	Just photos	100 µm	1	[197]
Crosslinked polyester-polyimide	SiO_2	T = 89.8 % Haziness 2.6 ua	50 nm	/	[198]
Polyacrylate	cloisite	T = 81 to 86%	100 µm	1 to 3	[192]

UNCORRECTED PROOF

Table 8
Transparent nanocomposites with magnetic properties.

Polymer matrix	Nanoparticles	Transparency	Thickness	NPs content wt.%	ref
Ion-exchange resin	γ-FeO_3	Just announced	/	/	[141]
PMMA	Fe oxide	photos	5 mm	0.01 to 0.065	[106]
silicone modified cycloaliphatic epoxy resin	Zr-resin	photos	/	/	[200]
cellulose	$MnZnFe_2O_4$	T(λ) = 40 to 80 %	20 µm	/	[201]

Table 9
Transparent nanocomposites with UV shielding properties. NPc is the NPs content.

Polymer matrix	Nanoparticles	Transparency	Thickness	NPs Content (wt.%)	Ref
PMMA	ZnO QDs	Photos	/	/	
		T(λ) = 70 to 90	40 mm	0.5	[102]
	ZnO	Just announced	/	/	[205]
		T > 95 % (UV-Vis)	1.5 to 2.5 µm	9.4	[204]
		Photos + Abs UV-Vis	45 µm	8	[161]
		T (550 nm) = 91 % (UV-Vis)	2 µm	Up to 11	[184]
		T(550 nm)> 80%	2 to 4 µm	0.5 to 2	[217]
		ZnO/PMMA not transparent	40 µm	/	[218]
		ZnO/Pu-PMMA transparent (photos)			
		T = 90 – 92 %	30 µm	0.2 to 0.8	[212]
	TiO_2	Just announced	/	/	[61]
PS	ZnO	Abs UV-Vis only	/	/	[81]
		T (NPc) from 40 to 80 % (UV-Vis)	64-68 µm	0 to 9	[216]
	TiO2	T< 80%	70 µm	/	[178]
		TiO2 grafted PS : T : 30 to 80%	70 µm	0.2 to 1.05	
		Abs UV-Vis only	100	4	[209]
	CeO2	T 60 to 80 %	2.5 µm	5	[37]
PVA	ZnO	T : 80 to 90 %	1 µm	1 to 3	[206]
	TiO2	T (λ, NPc) = 5 to 80 % UV-Vis + photos	100 to 200 µm	5 to 20	[79]
		Abs UV-Vis + visual observation	/	/	[208]
	FeS2	T 60 % photos	5 µm	/	[145]
PBMA	ZnO	T(λ)>90 to 94%	100 µm	5	[110]
PUA	ITO	From 60 to 90 % (λ and NPc)	100µm	0 to 9	[87]
PE	ZnO	Abs UV-Vis + photos	1µm	60	[207]
PP	ZnO	/	/	/	
PE-PVA copolymers	ZnO	Abs UV-Vis	0.1 to 1 mm	0.22 to 0.49	[146]
	TiO2	Abs UV-Vis	0.1 to 1 mm	/	
Epoxy matrix	ZnO	UV-Vis T(550 nm) >85%	/	0.07 to 0.15	[90]
		T < 70%	/	Up to 4	[219]
PS-PnBA	ZnO	T < 80%	64-68 µm	Up to 9	[215]
Silicon	ZnO	Abs UV-Vis only	/	1	[220]
PC	TiO_2	Abs UV-Vis only	100 µm	4	[209]
	Alumina nanowhiskers	T(λ) from50 to 80%	150µm	2	[111]
Polyacrylic	TiO_2	Just announced	200µm	0.6	[213]
Chitosan		T (λ, NPc) = 5 to 50 % UV-Vis	500 µm	1 to 10	[210]
Castor Oil resin	CeO_2	T(λ) from 40 to 80 % UV-Vis	40 µm	7	[211]
Poly-styrene sulfonate /poly(diallyl dimethyl ammonium)	Ce	T (λ n layers) = 80 to 92 % UV-Vis + photos	Up to 244 µm	12	[221]
PVP	FeS_2	T up to 90% UV-Vis + photos	1 µm	/	[145]
PVB	ZnO	99 % at 550 nm	/	1%	[63]

$$T_r = \frac{I_r}{I_0} \quad (8)$$

Where I_r is the intensity of the regular transmitted light by the composite and I_0 is the intensity of the incident light.

The transmitted light can be characterized more deeply by other analyses. By using a gonio-spectrophotometer, the transmitted light can be characterized as a function of angle. The characterization of the diffuse transmission brings new transparency parameters: the haze and the clarity. Haze characterizes wide angle scattering and results in loss of contrast of the object seen through the composite. Clarity characterizes narrow angle scattering and results in blurry images with no sharp details when looking through the composite. The origin of wide and narrow angle scattering in composites comes from the different types of light scattering by particles. Small particles scatter the light in all directions (wide angle scattering) whereas bigger particles favor the light scattering in the forward direction (narrow angle scattering). The scientific community commonly measures light transmittance and haze in general accordance to the standards ASTM D 1746 [45] and D 1003 [46], but some divergences persist for clarity measurements [47,48]. Clarity can be characterized by an-

UNCORRECTED PROOF

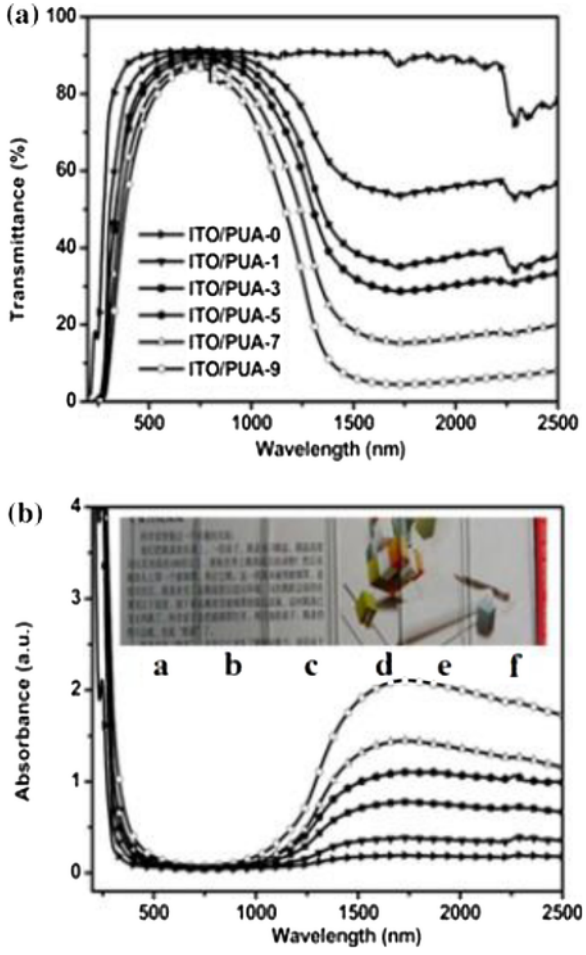

Fig. 4. UV–VIS–NIR spectra of ITO/PUA nanocomposites with different ITO contents (a) transmittance and (b) absorbance (the inset picture are digital photographs of 100 um thick ITO/PUA coatings on glass substrate containing 9 wt.%, 7 wt.%, 5 wt.%, 3 wt.%, 1 wt.% and 0 wt.% of the ITO NPS, respectively (A–F)). [87], Copyright 2014. Reproduced with permission from Elsevier Ltd.

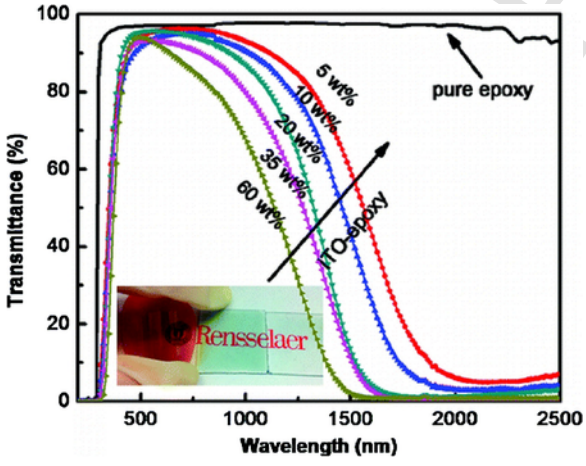

Fig. 5. Transmittance spectra of ITO/epoxy nanocomposite at different ITO content in the UV–vis-near IR - domain. [222], Copyright 2011. Reproduced with permission from the American Chemical Society.

gular dispersion methods as small angle scattering method [47,49] or by intensity measuring method depending on just one intensity value for ASTM D 1746 [45] or on more than one intensity values with Byk-Gardner Haze Gard Plus. Zhou et al. [47] carefully studied transmittance, haze and clarity of PC, PS, and PMMA nanocomposites. They showed how differences in refractive index between particles and matrix induced a decrease in both light transmittance and haze whereas larger particles affected the clarity. Psychophysical transparency characterization consists of determining the perceived appearance of composites, particularly the visual interaction with the fore- and background by examining the modification of contrast and sharpness of images seen through the composite. Generally, in transparent composite publications, the study of psychophysical transparency is underutilized and limited to a simple photograph of a composite laying over an image. Most of the time the sample is in contact with the background even though the appearance of composite can be completely different when the distance between the sample and the background increases (Fig. 1).

The interpretation of the perceived appearance of a composite is rather subjective and depends on the judgement of the observer. To understand and assess how the impression of a transparency is produced, several models of perceptual transparency have been developed, such as the arithmetic model [51], the luminance model [52] and the X-junction contrast-polarity model [53]. Kitaoka [54] connected the X-junction contrast-polarity model with the luminance-based arithmetic model. The X-junction contrast-polarity model can determine if an object is transparent by determining whether it is over or under another object of different color. Vahabi et al. [48] studied both the physical and psychophysical transparency of a nanocomposite made of PC filled with polyhedral oligomeric silsesquioxane. The psychophysical transparency was evaluated using the Kitaoka model. Differences were noted between physical and perceived transparency. The perceived psychophysical transparency resulted was higher than the measured physical transparency. Even though PC/silsesquioxane had better transmittance results than PC/silsesquioxane/ resorcinol bis (diphenyl phosphate), it had a milky aspect that was more pronounced and was therefore defined as translucent rather than transparent.

5. Nanocomposite fabrication methods

The dispersion of particles and their affinity with the matrix are crucial parameters that closely control global properties of nanocomposites. For an optimal transparency, nanocomposites require particles with dimensions very small compared to the wavelength ($D/\lambda<<1$). This condition can only be respected if primary particles are synthesized in such dimensions and if aggregation of particles is avoided. A challenge for nanocomposite fabrication is to incorporate well-dispersed isolated particles into the polymer matrix and to improve interfacial interactions between matrix and fillers. However, due to their high specific surface area and surface interactions often involving polar groups located at the surface, nanoparticles have a strong tendency to aggregate. These phenomena can be overcome by modifying the inorganic particles surface with organic compounds. The surface modification of inorganic particles can be performed through ionic exchanges with organophilic ions, physical adsorption or by chemical reactions with small molecules such as coupling agents, or polymer grafting. This enables minimization of interfacial energies between the polymer matrix and fillers, inducing a drastic enhancement of inorganic particles dispersion into the polymer matrix. The various methodologies for surface modification of inorganic nanoparticles will be discussed further in this review. Nanocompos-

CORRECTED PROOF

Table 10
Transparent nanocomposites with IR shielding properties. NPc is the NPs content.

Polymer matrix	Nanoparticles	Transparency	Thickness	NPs Content (wt.%)	ref
PMMA- PnBA	ATO	T(λ, NPc) : from 60 to 85 % UV-Vis	58 to 62 µm	3 to 10	
Epoxy matrix	Al doped ZnO	T(λ, NPc) : from 20 to 80% UV-Vis	3.5 mm	Up to 0.30	[88]
	Grafted ITO	> 80 % UV vis + photos	20 µm	5 to 35	[222]
Acrylic poyurethane	ITO	T(λ) from 80 to 90 % UV-Vis + photos	30 µm	5	[224]
		T(λ, NPc) from 60 to 90 % UV-Vis	100	0 to 9	[87]
Polu(thiourethane-urethane)urea	TiO_2	Just announced	80-100 µm	2.5 and 5 wt.%	[226]

Table 11
Transparent nanocomposites with coloration properties.

Polymer matrix	Nanoparticles	Transparency	Thickness	NPs Content (wt.%)	ref
	Si@Ag	Up to 95 % (abs in blue wavelength)	0.46 mm	/	[163]
PS	Au-PVP	Abs UV-Vis only	/	/	[229]
Teflon	Ag	Abs UV-Vis only	/	/	[230]
PVP	Ag	Abs UV-Vis only	/	/	[228]
PDMS	Ag Nanowires	T (λ) = 43 to 82 %	1 mm	/	[114]
PMMA	Rare earth	Abs UV-Vis only + photo	/	0.5 to 10	[232]

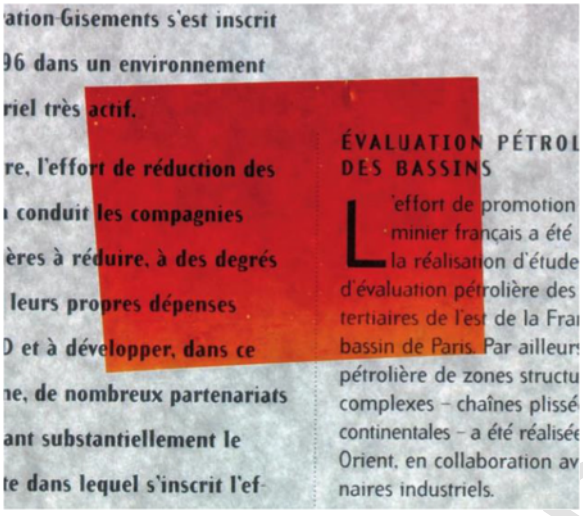

Fig. 6. Ag/PVP nanocomposites film with a heavily red color but keeping its transparency. [228], Copyright 2001. Reproduced with permission from John Wiley & Sons Inc. (For interpretation of the references to colour in this figure legend, the reader is referred to the web version of this article).

ites may be fabricated by several methods such as melt or solution blending of inorganic nanoparticles and polymeric matrix, in-situ polymerization, and/or in-situ particle formation. The purpose of this section is to describe these methods while providing examples of transparent nanocomposites for each fabrication technique [1,2,7,31].

5.1. Blending methodology

Direct mixing of particles or surface modified particles with the polymer matrix is the simplest method to synthesize nanocomposites. Two methods of blending can be conducted depending on the state of the polymer matrix: melt blending or solution blending. Melt blending consists of integrating particles in a melt polymer, while in solution blending the polymer matrix is solubilized in a solvent and particles are added to the solution. Melt blending may be accomplished by different processes such as extrusion, high shear mixing and thermal spraying. The main advantage of these processes is the large quantity of nanocomposites that can be manufactured, particularly with extrusion. Drawbacks of melt blending are the occasionally persistent poor dispersions of particles in the matrix and degradation of polymer matrix or surface modifiers due to high temperatures needed for melt processing. Only a few studies of melt blending with an internal mixer have been reported for transparent nanocomposites such as PC filled with surface modified alumina particles [55,56], surface modified organoclays introduced into either hydroxyl terminated polybutadiene [57], or ethylene-propylene-diene rubber [58] or polyethylene [59] polymer matrices. In this technique, the polymer matrix is first melted in the mixer under the relevant controlled temperature, the fillers are then added in the mixer and the dispersion of particles is performed by spinning rotors. The use of an internal mixer is often limited to the compounding of master-batches that are subsequently extruded. Extrusion is the compounding technique most used for thermoplastics. Among the different types of extruders, co-rotating twin screw extruders are the most adapted to compound thermoplastic matrix with inorganic fillers. The presence of two screws enables better mixing and better particle dispersions are obtained. Particles can be directly inserted with the polymer in the main hopper placed at the beginning of the barrel or particles can be inserted separately in a side hopper placed further in the barrel. The processing parameters such as melt temperature, screw profile, and screw speed have a huge influence on the final dispersion and properties of the compounded nanocomposites. In the nanocomposite literature, a wide range of thermoplastic matrices with various inorganic particles have been fabricated by extrusion. More precisely, transparent nanocomposites of PC filled with surface modified silica particles [60] or polyhedral oligomeric silesquioxane [48] have been obtained via extrusion processing. PMMA/TiO_2 [61], poly(ethylene terephtalate)/TiO_2 [62], poly(vinyl butyral)/ZnO [63], low density polyethylene and poly(ethylene-co-butyl acrylate) filled with TiO_2, ZnO and SiO_2 particles [64] were also prepared by extrusion and formed transparent nanocomposites. Clay fillers have been widely extruded with polymer matrices and showed delamination of clay layers due to polymer intercalation [1]. Transparent nanocomposites filled with clay fillers have been extruded with different polymers: PC [65,66], PMMA [67,68], poly(vinyl chloride) [69], poly(L-lactic acid) [70], xanthan-starch [71] and low density polyethylene [72–74]. Though less frequently used, the thermal spray was revealed to be an efficient process for surface coating. Particles and polymer matrix are mixed, heated and projected onto a surface. Singhal and Skandan [75] used thermal spray process to obtain a transparent hard coating made of ceramic

UNCORRECTED PROOF

Table 12
Transparent nanocomposites with extreme refractive index. NPc is the NPs content.

Polymer matrix	Nanoparticles	Transparency	Thickness	NPs Content (wt.%)	ref
PMMA	TiO_2	T > 90% (UV-Vis) + photos	200µm	/	[239]
		T(λ, NPc) : from 55 to 80% UV-Vis	2.35 µm	From 1 to 5	[245]
Poly(hydroxydiethoxylate bisphenol-A dimethacrylate-co-dodecyl methacrylate)	Yb3+:CaF_2	T(λ) : from 30 to 77% UV-Vis	2 mm	84	[113]
PVA	TiO_2	Abs Uv-vis + visual observation	40-80µm	2-35	[208]
Epoxy	TiO_2	T (e, NPc) from 83 to 95 %	25 to 85 nm	10 to 30	[98]
		T (e, NPc)from 90% to 100 %	1.5 to 3.4 µm	10 to 40	[235]
PHE	TiO_2	T> 85 % UV-Vis	1 µm	0 to 80	[236]
Polyimide	TiO_2	Abs UV-vis only	276 to 1021 nm	Up to 40	[237]
		T(λ, NPc) from 61 to 91 %	20 µm	Up to 50	[238]
		T(λ, NPc) from 85 to 92 %	500-600 nm	Up to 50	
	ZrO_2	T(λ, NPc) from 74 to 91 %	20 µm	Up to 50	
		T(λ, NPc) from 88 to 92 %	500-600 nm	Up to 50	
		T(λ, NPc) from 70 to 92 %	19 µm	Up to 50	[241]
		T(λ, NPc) from 88 to 95 %	500-600 nm	Up to 50	
Styrene and Maleic anhydride copolymer	TiO_2	Just announced		40	[236]
Silicon	TiO_2	T from 70 to 90 % UV-Vis + photos	5 mm	From 10 to 20	[96]
		T(λ, NPc) : from 80 to 92% UV-Vis	/	From 10 to 30	[246]
poly(4-vinyl benzyl alcohol)	TiO_2	T> 85 % for λ > 500 nm	50 µm	60	[86]
caprylic capric triglyceride	ZnO	T(λ, NPc) : from 50 to 92% UV-vis (+ integrating sphere)	20 µm	0 – 60	[240]
Gelatin	Au	not studied	200-400 µm	up to 48	[244]
	PbS	not studied	40 nm to 2 µm	up to 82	[243]
Polythiourethane (PTU)	PbS	T(λ, NPc) : from 62 to 95% UV-Vis	1 µm	17 and 37	[234]
PUrMA	ZnS	> 90 %	1 µm	Up to 86	[99]
PVD-PDMAm hydrogel	ZnS	Photos only	3-10 mm	Up to 60	[247]
Fluorinated polyimide	2D fluoro-graphene	T>90%	3 µm	0.25 to 1	[182]
Thiol-acrylate Resin	TiO_2/ZrO_2	T(λ, NPc) : from 85 to90 % UV-Vis	4-6 µm	Up to 80	[248]
PITE	TiO_2	T(λ, NPc) from 55 to 90 %	20 µm	Up to 50	[242]
		T(λ, NPc) from 80 to 92 %	500-600 nm	Up to 50	
	ZrO_2	T(λ, NPc) from 56 to 90 %	20 µm	Up to 50	
		T(λ, NPc) from 84 to 94 %	500-600 nm	Up to 50	

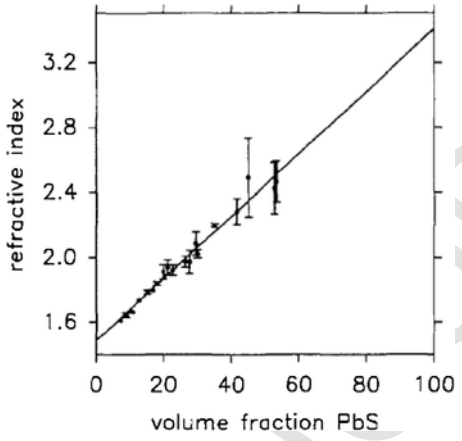

Fig. 7. Linear evolution of the refractive index of a gelatin matrix with the volume fraction of PbS fillers. [243], Copyright 1993. Reproduced with permission from Elsevier Ltd.

particles and polymer matrix. Solution blending is a simple process involving the dispersion of particles in a solution containing the solubilized polymer matrix. The fundamental condition for the use of this technique is an appropriate choice of solvent combining the good solubility of the polymer matrix with the dispersibility of nanoparticles. In most instances, particles require surface modification to be well dispersed in organic solution. The particle dispersion can also be improved with an ultrasonication step. For nanocomposites filled with fibers, the solution blending process might be preferred because the stress applied is less important, contrary to high shear processes such as extrusion which breaks fibers and decreases their size. Solution blending is used extensively for the formation of nanocomposite films. Films are easily obtained by combining solution blending with processes such as printing, film casting, dip coating and spin coating. All these methods consist of the deposition of the particles/ polymer solution into a mold or onto a substrate and after evaporation of the solvent the nanocomposite is obtained. Spin coating is widely used to prepare nanocomposite films of typical 1–100 nm thickness. The blended solution is dropped onto the substrate. Under a high-speed, controlled rotation of the substrate, the polymer/nanoparticle solution spreads and after a fast evaporation of the solvent, a homogenous film is recovered. Drawbacks of solution blending are the cost of the solvent and its potential toxicity due to evaporation. Examples of polymer/clay transparent nanocomposite films were prepared by mixing organo-modified clays with either poly(methyl methacrylate) in N-methyl-2-pyrrolidone, [76] or with soluble fluorinated polyimide in *N-N*-dimethylacetamide solvent [77]. Parlak and Demir [37,78] synthesized transparent nanocomposites by solubilizing PS in tetrahydrofuran in the presence of surface modified ceria nanoparticles. The solution was spin-coated to provide films with a thickness of 2.5 µm. Mallakpour et al. [79,80] combined solution blending and solution casting to form two types of transparent nanocomposites from solutions of polyvinyl alcohol in ethanol mixed either with modified TiO_2 [79] or modified $Al2O_3$ [80] particles. Unmodified ZnO and SiO_2 particles were dispersed in polystyrene/*N,N*-dimethylac-

UNCORRECTED PROOF

Table 13
Transparent nanocomposites with photoluminescent properties. NPc is the NPs content.

Polymer matrix	Nanoparticles	Transparency	Thickness	NPs Content (wt.%)	ref
PMMA	ZnO	Abs UV-Vis + photos	45 µm	8	[161]
	ZnO QDs	T(λ) = 70 to 90	40 mm	0.5	[102]
		T : 80- 90 %	100 µm	0.5 to 3	[251]
	ZnO	/	/	/	[252]
	CdS	Abs UV-Vis only	/	7	[183]
	Mn doped ZnS	80 to 90 %	10 mm	1.1	[250]
	GdOF:Ce,TB [257]	T(λ, NPc) : from 30 to 75% UV-Vis	3 mm	0.032 to 1.5	[109]
	Doped CeF3	T(λ, NPc) : from 20 to 97% UV-Vis	0.1 mm	Up to 20 vol%	[25]
	CdS@ZnS	T 55 % (photos andUV-Vis)	/	/	[253]
Epoxy Matrix	ZnO QDs/SiO_2	T(λ, NPc, thickness) = 10 to 85	Up to 4mm	1 to 15	[92]
	ZnO QDs/SiO_2	Just announced			[33]
Poly(butanediol monoacrylate)	ZnO	T : 90% UV-Vis	/	10	[84]
Silicon	ZnO-SiO2	T(λ, NPc) : from 50 to 80% UV-Vis	0.5 mm	1 to 5	[34]
	PDMS-CdSe QDs	T(λ): from 20 to 80 UV-Vis	400 µm	0.2	[254]
PHEMA	ZnO	Photos only	/	/	[101]
PS	ZnO	Abs UV-Vis only	/	/	[216]
	CdTe	Photos only	/	/	[100]
	Doped CeF3	T(λ, NPc) : from 30 to 75% UV-Vis	0.1 mm	Up to 20 vol%	[25]
PVA	CdS	Abs UV-vis only			[143]
		T(λ) : from 65 to 85 %	/	/	[249]
	ZnO	T(λ, NPc) : from 80 to 90% UV-Vis	1 µm	Up to 3	[206]
	YAG:Ce3+	T from 85 to 90 % UV-Vis + photos	/	21.1	[255]
PVP	YAG:Ce3+	T from 85 to 90 % UV-Vis + photos	/	34.7	[255]
PA	Epoxy funct. Y-Al2O3	Abs UV-Vis only	/	/	[256]
PMMA	ZnO QDs	Photos only	/	/	[257]

Table 14
Transparent nanocomposites with dichroism and non linear optical properties.

Polymer matrix	Nanoparticles	Transparency	Thickness	NPs Content (wt.%)	ref
PE	Au	Abs UV-Vis only	0.3 mm	2	[258]
	ZnO	ABS UV-Vis only	1 µm	From 3 to 16 wt%	[261]
PMMA	TiO_2	Just announced	/	/	[264]
		80-90 % at 780 nm, "transparent to the eye"	250 to 350 nm	Up to 60 wt%	[262]
		Abs UV-Vis only	/	/	[263]
PS	CdS	Just announced	/	2 to 17	[147]

etamide [81] and polyamide/formic acid [82] solutions, respectively. Transparent nanocomposites were produced after solution casting.

5.2. In situ polymerization in the presence of inorganic nanoparticles

In-situ polymerization is based on the dispersion of the inorganic particles in the monomers or in the mixture of monomer and solvent prior the polymerization step. The modification of the surface of inorganic particles is crucial in this process as the organic functional groups enable a better dispersion of the particles in monomer which is essential for in-situ polymerization. Thanks to the easy dispersion of particles via this process, the in-situ polymerization method has been widely used to fabricate transparent nanocomposites. Thermal radical polymerization and photo-polymerization associated with cross-linking are common techniques employed for in-situ polymerization. Transparent nanocomposites of various compositions were synthesized by in-situ radical polymerization. Either crude inorganic nanoparticles or modified inorganic nanoparticles were dispersed in monomer(s) prior to starting the polymerization. Examples of transparent nanocomposites prepared by in-situ thermally-or photo-initiated radical polymerization of monomers in the presence of nanoparticles are summarized in Table 1. For example, surface modified ZnS particles were dispersed in a mixture of styrene, *N,N*-dimethylacrylamide and divinylbenzene. The resulting mixture was exposed to γ-ray irradiation to conceive transparent nanocomposite [83]. Other examples reported photo-initiated free radical polymerization to produce polyacrylic-based nanocomposites filled by either ZnO [84], SiO_2 [85], or TiO2 [86]. For example, the radical polymerization of either vinyl benzyl alcohol monomer or ethoxylated (6) bisphenol A dimethacrylate was performed in the presence of TiO2 nanoparticles functionalized by different ligands to produce a series of nanocomposites with different levels of transparency (acrylic acid, hexanoic acid or benzylic acid) [86]. It is worth mentioning that the rate of vinyl benzyl alcohol polymerization is higher for acetic acid-surface functionalized TiO2 in comparison with phenyl acetic acid-TiO2 [86]. This was rationalized by a higher steric hindrance [86]. The highest level of transmittance of 80% was observed for poly(vinyl benzyl alcohol) loaded with 60 wt-% of acetic acid-TiO2 nanoparticles [86]. Interestingly, polyurethane-based transparent nanocomposites were synthesized by radical copolymerization of an oligo(urethane acrylate) monomer and 3-(trimethoxysilyl)propylmethacrylate functionalized tin-doped indium oxide (ITO) particles [87]. The fabrication of nanocomposites was also implemented via the dispersion of inorganic particles with epoxy precursor followed by the addition of a cross linking agent and post-curing step. Epoxy resin-based transparent nanocomposites were achieved by this method with the embedding of a variety of inorganic nanoparticles: surface modified Al-doped ZnO [88], modified ZrO_2 [89], ZnO [90,91], SiO_2-TiO_2

UNCORRECTED PROOF

[19,80,15], ZnO-SiO_2 [81,15] and SiO_2-TiO_2-SiO_2 [91], ZnO [93], colloidal mesoporous silica [94] or Bentonite clay grafted with poly(glycidyl methacrylate) chains ([95]). In a similar approach, TiO_2 was also dispersed in silicon resin [96], polyester resin [97], or epoxy resin [98] to realize transparent nanocomposites by in-situ polymerization.

5.3. In situ particle formation in preformed polymer matrix

In situ particle formation is obtained by synthesizing inorganic particles in the polymer matrix. The particles formation can be carried out through various synthesis techniques such as sol-gel process, chemical reductions, photoreductions and thermal decomposition of particle precursors, either in the presence of the polymer or directly in monomer(s). As detailed in the examples of the following parts, the simultaneous formation of both particles and polymer matrix led to highly homogeneous nanocomposites. The challenge of in-situ particle formation resides in avoiding phase separation between organic and inorganic phases during the synthesis. Different interactions favor a better phase compatibility, e.g., hydrogen bond interactions, ionic interactions, π-π interactions and covalent bonds.

The sol-gel process is an effective method to synthesize various inorganic oxide particles. An organometallic precursor is hydrolyzed and condensed to form the final inorganic particle. The most current precursors are tetraethoxysilane (TEOS) and tetramethoxysilane (TMOS) for the synthesis of silica particles, tetrabutyl titanate for the synthesis of titania particles and aluminum isopropoxide for the synthesis of alumina particles (Table 2) [2,7]. The sol-gel process in most of the cases is conducted in water/alcohol solvent but it can also take place in organic solvent such as tetrahydrofuran (THF), *N,N*-dimethylformamide (DMF), dimethyl sulfoxide (DMSO) and dimethyl acetamide (DMAc). Acid and base catalysts are often used to raise the reactivity of metal alkoxide in the sol-gel process. An acid catalyzed sol-gel process has a fast hydrolysis step and that results in an open weakly ramified inorganic network. On the contrary, a base catalyzed sol-gel process undergoes slow hydrolysis and fast condensation steps leading to the formation of compact particles [43]. The formation of transparent nanocomposites via in situ sol-gel has been intensively studied especially for transparent nanocomposites filled with silica nanoparticles. Transparent nanocomposites have been widely fabricated by the hydrolysis-condensation of TEOS or TMOS precursor in hydrogen bonding accepting polymer matrices (in all the following examples, the matrix was first solubilized in an adapted aqueous or organic solvent) such as PMMA [115,116], poly(vinyl alcohol) [117,118], Poly(vinyl acetate) [115,119], poly(2-methyl-2-oxazoline) [120,121], poly(*N*-vinyl pyrrolidone) [115,121], poly(*N,N*-dimethyl acrylamide) [115,121], polyamide 6.6 [122], cellulose acetate [123], modified chitosan [124], poly(dimethoxysiloxane) [125], polyethersulfone [126] and modified polyphosphazene [127,128]. Other interactions than H-bonding between inorganic and organic phase, have been reported in transparent nanocomposites synthesized via the sol-gel of TEOS or TMOS alkoxysilane precursors. Tamaki and Chujo [129] achieved the synthesis of transparent poly(styrene sulfonate)/SiO_2 nanocomposite via the sol-gel of TMOS and 3-aminopropyltrimethoxysilane precursors in a solution of poly(styrene sulfonate) in dimethyl sulfoxide. The amino groups of the inorganic particles exhibited strong anion-cation interactions with the polymer matrix. Tamaki et al. [130] also reported a transparent polystyrene/silica nanocomposite obtained via in situ sol gel of phenyltrimethoxysilane in THF solution of polystyrene. The homogeneity was found to be enhanced by π-π interactions between phenyl groups of polystyrene and the phenyltrimethoxysilane functionalized silica. Hsiue et al. [131] obtained a transparent nanocomposite with improved compatibility between polyimide and silica by condensing the phenoxysilane precursor in the polyimide to achieve silica nanoparticles functionalized with phenoxy groups. The presence of those phenoxy groups increased the compatibility between organic and inorganic phases. Nunes et al. [132] used strong interactions between amine and imide groups to improve the homogeneity of a transparent nanocomposite made of polyether imide and silica nanoparticles. The silica nanoparticles were synthesized by sol-gel of TEOS and aminoalkoxysilane precursors in the presence of the polymer matrix. Another effective method to improve organic/inorganic interactions is to form covalent bonds between the functional groups of polymer matrix and the inorganic particles. Vinyl monomers such as styrene, methyl methacrylate and acrylonitrile were directly copolymerized with 3-trimethoxysilylpropylmethacrylate to afford an alkoxy-silane reactive function to the polymer matrix [133]. Then, transparent nanocomposites were obtained by using those functional polymers for in-situ sol-gel process with [133–135] or without [136] addition of other alkoxysilane as described in Fig. 2.

The implementation of the sol-gel process in the presence of a polymer matrix for the fabrication of transparent nanocomposites was also reported for other metal alkoxides. Different transparent nanocomposites were obtained by in-situ hydrolysis-condensation of titanium precursors in different polymer matrices such as poly(dimethylsiloxane) [125], modified polyphosphazene [128], poly(amide-imide) [137], copolymers of 3-trimethoxysilylpropylmethacrylate with methyl methacrylate, of styrene and acrylonitrile [133] and of styrene with maleic anhydride [138]. Similarly, in-situ sol gel reaction from aluminum precursor were performed in transparent polymer matrix such as poly(vinyl alcohol) [139], modified polyphosphazene [128], copolymers of 3-trimethoxysilylpropylmethacrylate with methyl methacrylate, styrene and acrylonitrile [133]. Zirconium precursor was hydrolyzed and condensed in PMMA [135] and modified polyphosphazene [128], zinc precursor was used for in-situ sol-gel process in transparent poly(N-vinyl pyrrolidone) matrix [140].

Metal reductions and thermal decomposition of metal precursors were applied to synthesize inorganic nanoparticles inside polymer matrices. Ziolo et al. [141] synthesized a transparent nanocomposite filled with γ-Fe_2O_3 particles by precipitation and ion exchange between Fe(II) and a ion-exchange matrix composed of poly(styrene sulfonate) crosslinked with divinylbenzene. Porel et al. [142] obtained transparent nanocomposites of polymer matrix with silver and gold particles via reduction and thermal treatment of silver nitrate and chloroauric acid in polyvinyl alcohol (PVA) matrix. First, they solubilized the metal salt and polymer in an aqueous solution, then they spin coated the solution to form a thin film and finally they proceeded to a thermal treatment of the film. The PVA matrix acted as stabilizer and reducing agent for metal salts. Other inorganic nanoparticles such as cadmium sulfide (CdS) [130,131], lead sulfide (PbS) [144] or nanocrystalline iron sulfide [145] were synthesized in the polymer matrix to take profit of the specific properties of these semi-conductor particles such as fluorescence, nonlinear optical properties or UV-shielding.

5.4. Simultaneous in situ particle and polymer matrix formation

The simultaneous formation of both particles and polymer matrix is considered to be the most effective method to produce homogeneous nanocomposites. This technique involves the competition between three processes: i) the kinetics of inorganic particle formation; ii) the kinetics of polymerization of the organic monomers; and iii) the thermodynamics of phase separation between organic and inorganic phases. The phase separation can be avoided if the formation of

UNCORRECTED PROOF

both particles and polymer is simultaneous and fast. Another way to avoid phase separation is to favor attractive interaction between organic and inorganic phases. Transparent nanocomposites have been realized by coupling in-situ particle formation via sol-gel process and in-situ polymerization via different polymerization techniques (Table 3). To achieve transparent nanocomposite, the sol-gel process of TEOS or TMOS was combined with different polymerization routes such as radical polymerization of 2-hydroxyethylmethacrylate [148,149] and various acrylate monomers [150], ring-opening polymerization of cyclic alkenyl monomers [123], polycondensation of phenylene diamines and terephtaloylchloride (leading to aromatic polyamide) [151], crosslinking of epoxy and polyoxypropylene diamine [152], reactions between cyclic intermediate of polyimide and photopolymerization of various acrylate monomers [154]. Similarly, titanium isopropoxide was used as precursor for the formation of TiO_2 nanoparticles via sol-gel process with the synchronous radical polymerization of methyl methacrylate and trimethoxysilylpropyl methacrylate. This resulted in a transparent nanocomposite of PMMA filled with TiO_2 nanoparticles [155]. Inverse microemulsions have proved to be an interesting method to synthesize transparent nanocomposites in one step [10]. An inverse microemulsion is constituted of 2–20 nm diameter water droplets stabilized by surfactants dispersed in an oil phase. Inorganic particles can easily be synthesized by different processes in water droplets acting as nanoreactors. If the oil phase is pure monomer(s), the continuous organic phase can be polymerized to directly form a nanocomposite. Palkovits et al. [156] synthesized transparent nanocomposite of PMMA/silica by a single inverse microemulsion approach. Silica nanoparticles (26 nm) were obtained by sol-gel process in water droplets dispersed in methyl methacrylate monomer. The dispersion was then polymerized by thermally-initiated radical polymerization. Pavel and Mackay [157] achieved the fabrication of transparent nanocomposite by a multi-reverse microemulsion approach. Two separated inverse microemulsions containing Cd^{2+} and S^{2-} dispersed in a methyl methacrylate continuous phase were mixed together. After thermally-initiated radical polymerization of the monomer phase, a transparent nanocomposite of PMMA/CdS was obtained. Reduction and thermal decomposition of metal precursors have been conducted simultaneously with the formation of polymer matrix to design nanocomposites. Nakao [158] synthesized transparent nanocomposites of PMMA matrix filled with noble metals such as palladium, platinum, silver, and gold nanoparticles. For this, thermal decomposition of metal precursors was combined with simultaneous radical polymerization of methyl methacrylate. Balan and Burget [159] obtained a transparent nanocomposite by coupling photopolymerization of different acrylate monomers with in situ formation of bismuth nanoparticles via reduction of bismuth chloride (see Table 3). Akhavan et al. [160] reported PMMA/silver transparent nanocomposites synthesized by simultaneous silver ion reduction and methyl methacrylate γ-ray polymerization. PMMA/ZnO nanocomposites were designed in two steps via the first synthesis of PMMA/ZnO precursors by radical copolymerization of zinc methacrylate ($Zn(MAA)_2$) in ethanol solution with MMA followed by the bulk polymerization of MMA in a second step [102].

5.5. Casting of polymer solution loaded with core-shell nanoparticles

Core-shell particles were in polymer matrices to develop transparent nanocomposites via a direct mixing of the core-shell particles and the polymer solution prior casting and solvent evaporation. Inorganic-inorganic core-shell particles like CeO_2@SiO_2 or SiO_2@Ag were used to combine properties of both inorganic phases [153,154] but more interesting is the modification of the surface of inorganic nanoparticles by an organic layer to promote the dispersion of the nanoparticles inside the polymer matrix (Table 4) [66,45,155,26,156,50]. Controlling the dispersion of inorganic nanoparticles into a polymer matrix is essential and represents the main challenge in the nanocomposite fabrication from pre-formed nanoparticles and polymers. As a result of the high specific surface area of the nanoparticles and the gap between the interfacial energies of both the inorganic nanoparticles and the polymer matrices, inorganic particles have a strong tendency to aggregate. This aggregation hampers optimal nanoparticle dispersion into the matrix and deeply affects the nanocomposite properties. The surface modification of the inorganic nanoparticles by organic compounds is a way to minimize interfacial energies between inorganic particles and the polymer matrix. The surface modification of inorganic nanoparticles can be performed through the tethering of small organic molecules (coupling agents, compatibilizers) or by grafting polymer chains. The functionalization of inorganic nanoparticles by grafted polymer chains allows for the synthesis of hybrid core@shell nanoparticles and offers a wider range of possibilities to design functional surfaces with thicker organic shells. Since most often the surface of inorganic nanoparticles is covered by hydroxyl groups, covalent bonds can be formed through hydrolysis-condensation reaction with alkoxysilane-based molecules. Among the different silane coupling agents, the 3-(meth)acryloxypropyltrimethoxysilane has been widely used to modify the surface of SiO_2, Al_2O_3, TiO_2, ZnO, CeO_2 and other inorganic nanoparticles [66,45]. The head group of the modifier can be tethered to inorganic surface through physical adsorption or chemical reaction. Anchoring groups such as thiols (R-SH), amine (R-NH_2), carboxylic acid (R-COOH), phosphoric acid (R-$PO(OH)_2$) or sulfonic acid (R-SO_2OH) groups were involved in coordinative, electrostatic or hydrogen bonds with the inorganic surface. [1] In the studies devoted specifically to transparent nanocomposites, the polymer brushes of the core@shell nanoparticles were anchored by either "grafting onto," [156 155] "grafting through" [37] or "grafting from" [60] methodologies. The principle of these methodologies was described in different reviews [157,158]. Briefly, the principle of "grafting onto" is based on the coupling between an end-functionalized polymer and a functional group anchored on the inorganic surface while "grafting through" consists of grafting a vinylic monomer onto the surface that would be copolymerized during the polymerization of free monomer to create a mixture of free and bonded polymer chains. The "grafting from" strategy relies on the grafting of an initiator able to initiate the polymerization of free monomers from the surface of the particle. When combined with controlled polymerization techniques, the "grafting from" approach ensures a simultaneous initiation of all polymer chains. As a result, the high polymer grafting density induces polymer stretching [157,158]. The design of core@shell particles to match the refractive index between the loaded particles and the surrounding transparent matrix through the refractive index of the shell has proven to be a promising approach to reduce light scattering (Eq 2) and ensure transparency. This methodology has been mainly investigated with cerium oxide nanoparticles modified with either silica or poly(methyl methacrylate) outer shell to match the refractive index of polystyrene matrix [153,26].

It should be mentioned that several of theoretical and experimental studies were conducted on the investigation of the dispersion state of core@shell polymer@inorganic nanoparticles into polymer matrices. In these studies, the grafted polymer was similar to the polymer of the matrix, and was not specifically chosen for its transparency. However, the conclusions drawn from these studies regarding the parameters affecting the quality of the core@shell nanofillers dispersion inside polymer matrix is very instructive for the design of transparent

UNCORRECTED PROOF

nanocomposites. In a general trend, the dispersion of polymer grafted nanoparticles into polymer matrices is affected by three main parameters: the grafting density of the polymer chains on the nanoparticles surface (σ), the molecular weight of the grafted chains (N) and the molecular weight of the free chains (P). A parameter of great concern defining the dispersion state of the particles is the threshold value of the ratio R = N/P for which the nanoparticles go from a well dispersed state to an agglomerate state. Such transition is also called the wet to dry transition. The pioneering works of De Gennes [166] predicted a transition at N = P (R = 1) for polymer brushes grafted onto flat surfaces. Experimentally, it has been shown that this value is lower for brushes grafted onto spherical nanoparticles due to a curvature effect [167–169]. Chevigny et al. [169] investigated the dispersion state of PS grafted silica nanoparticles in a PS matrix. The polymer grafted particles were synthesized by coupling a grafting from technique and a nitroxide-mediated controlled radical polymerization. The authors paid particular attention to controlling the colloidal stability during the synthesis to avoid aggregation. Individual nanoparticle dispersions were obtained for R > 0.24 whereas for R < 0.24 large and compact aggregates were obtained. This shift of the wet/dry transition in comparison to flat brushes was ascribed to the effect of surface curvature. It could also be ascribed to processing kinetic effects and the polymer polydispersity. A significant collapse of the grafted chains was observed for the aggregate state (R < 0.24). Sunday et al. [168] coupled the "grafting from" technique with controlled radical polymerization to graft polystyrene chains onto silica nanoparticles. A phase diagram was developed to predict the dispersion state of grafted nanoparticles in polymer matrices considering σ and the swelling ratio (=P/N). At both very low and very high grafting density, the nanoparticles formed aggregates in the matrix. This can be explained at very low grafting density by the allophobic wetting transition due to inorganic core-core attractive interactions, while at very high grafting density the autophobic wetting transition takes place due to large conformational entropic penalty inducing an expulsion of the matrix chains from the brush layer [170]. At intermediate grafting density, the interactions between grafted and free chains govern the dispersion state of the nanoparticles and two cases may present. If the free chains are larger than the grafted chains, unfavorable mixing entropy leads to an expulsion of the matrix chains from the grafted shell resulting in important aggregations of the nanoparticles. Nevertheless, if the molecular weight of the anchored polymer chains is higher than the matrix chains, the mixing entropy promotes a complete wetting of the grafting chains by the free chains resulting in well dispersed nanoparticles. To minimize the free energy of the system, grafted chains undergo a compression when N < P, and an extension when N > P [169]. Sunday et al. [168] observed a similar wet/dry transition value, at equivalent grafting density and comparable systems. Chevigny et al. [169] and Kumar et al. [12] gathered in a review all the available data found in the literature concerning nanoparticle morphologies observed in polymer matrices filled with polymer grafted inorganic nanoparticles to build a morphology diagram. The data was related to silica or magnetic nanoparticles of similar sizes and different grafted polymers (PS, poly(n-butyl acrylate) and poly(ethylene oxide)). A general consensus emerging from all these investigations is that the dispersion state of core@shell polymer@inorganic particles in polymer matrices depends on a subtle balance between entropic and enthalpic interfacial interactions. Well-dispersed nanoparticles can only be obtained for a restrictive range of polymer grafting densities and molecular weight of grafted and free chains. The research group of Pr. Benicewicz enlarged this range of combinations considerably, leading to well-dispersed nanoparticles in polymer matrices by grafting bimodal brushes on inorganic nanoparticles [12,96,170,171]. A bimodal brush is defined as a homopolymer brush made of two distinct lengths of grafted chains. If both types of chains exhibit different chemical nature, the appropriate term is then a mixed bimodal brush. The strategy of the Benicewicz research group was to graft short polymer chains with a high grafting density to screen the enthalpic core-core attractions while simultaneously grafting long polymer chains with a low grafting density to enhance entanglement and the wetting of the long grafted chains by the matrix polymer chains [170,171]. The grafting of these bimodal polymer brushes on inorganic nanoparticles led to well-dispersed particles even in entropically unfavorable higher molecular weight matrices. The mechanical properties [170,171] (storage and elastic modulus, hardness, Tg) or the transparency [96] of the nanocomposite filled with bimodal brushes grafted nanoparticles were greatly enhanced in comparison to nanocomposites filled with monomodal brush grafted nanoparticles. These improvements were the result of a better dispersion state of the core@shell nanoparticles and favored interactions (entanglements) between grafted and free chains.

6. Properties of transparent nanocomposite and applications

The incorporation of inorganic nanoparticles into polymer results in nanocomposites with enhanced or new properties such as mechanical, optical, thermal, barrier or magnetic properties. The improvement of those properties is dependent on nature, size, dispersion, percentage of incorporation of the filler and on the interfacial interactions between the polymer matrix and the inorganic particles. The addition of inorganic particles into polymer can enhance several properties at the same time. For example, the addition of CeO_2 nanoparticles into PMMA matrix can simultaneously enhance mechanical strength, UV filtering and thermal stability. For clarity, the studies will be introduced according to the targeted property of the polymer nanocomposite in addition to the claimed transparency. For each given property we draw a table providing the polymer matrix, the type of nanoparticles used, their incorporation rate, the thickness of the sample and the quantitative level of transparency with characterization methods when provided in the different studies. Depending on the targeted application for polymer nanocomposites, the required level of transparency differs. Mostly, for the nanocomposites fabricated for optical applications (such as UV- or IR- filtering, high refractive index materials, optoelectronics, color generation or photoluminescence), transparency is a key parameter. Transparency is also valued for polymer nanocomposites with barrier properties, for example in food packaging applications. For the other applications reported in this review such as mechanical, thermal or magnetic properties, the significance given to the transparency criteria will be given in the corresponding tables.

6.1. Mechanical properties

Enhancing the mechanical properties such as Young's modulus, toughness, hardness, tensile and flexural strength, abrasion and scratch resistance or ductility, is frequently the main reason to add inorganic particles into a polymer matrix. The mechanical behavior of inorganic/polymer transparent nanocomposites has been extensively studied as reported in Table 5. Different trends can be identified concerning the enhancement of the different mechanical properties according to the nature of the filler and the matrix, the filler concentration and the interfacial interactions between matrix and fillers. Several investigations reported that transparent nanocomposites made of unmodified inorganic particles (e.g., SiO_2, TiO_2, ZnO, ZrO_2, alumina and clay) and polymer matrices exhibited mechanical reinforcement

UNCORRECTED PROOF

[73,94,115,127,128,137,172] even at low loading of fillers (<5 wt%) [61,170] but also showed some limits due to aggregations or weak interfacial interactions. Nakane et al. [118] studied the mechanical behavior of a transparent composite of poly(vinyl alcohol) filled with silica. With filler content of 30 wt%, the Young's modulus was drastically increased while the elongation at break decreased and the composite became more brittle. Similar mechanical behaviors were observed by Sengupta et al. [122], Sarwar et al. [174] and Chae et al. [81] for transparent composite of poly(amide-6.6)/SiO_2, poly(trimethylhexamethylene terephthalamide)/SiO_2 and PS/ZnO, respectively. The poly(amide-6.6) matrix filled with 5 wt% of SiO_2 nanoparticles improved storage, Young's modulus, and tensile strength but the brittleness increased for silica loading above 10 wt%. The poly(trimethylhexamethylene terephthalamide) exhibited higher mechanical strength with the addition of 10 wt% of silica but the elongation at break and the toughness decreased, while the brittleness of the composite increased at loading above 25 wt%. A significant enhancement of the tensile modulus was noticed for PS matrix when 5 wt% of ZnO particles were added, whereas the elongation at break was decreased. The interfacial adhesion was not strong enough to withstand large mechanical forces. Evora et al. [97] reported that the toughness of transparent polyester/TiO_2 composite increased by 57% for low particle loading of only 1 wt% but the toughness value almost decreased to the toughness value of the neat polymer matrix for particle loading of 4 wt%. This decrease was ascribed to particle agglomeration. Many publications revealed the importance of targeting the optimal dispersion state and strong interfacial interactions between inorganic particles and polymer matrix to improve hardness [91,98,175,166], scratch resistance [103], wear resistance [178] or mechanical strength [58,69,76,89,112,125,131] of transparent nanocomposites. Surface modification of particles or the use of compatibilizers are often required to achieve any gain in mechanical properties. Hakimelahi et al. [111] modified the surface of alumina fillers by grafting PC chains via in-situ polymerization. The PC modified alumina fillers were then dispersed in a methylene chloride solution of PC. A transparent nanocomposite was finally obtained by solution casting. In comparison to the pure polymer, the tensile strength and the Young's modulus were enhanced for composites with the modified fillers. On the contrary, no improvement of properties was noticed for composites filled with the raw particles. In comparison, Inceoglu et al. [74] fabricated a starch-clay/low density polyethylene transparent composite via melt blending. They studied the influence of a maleic anhydride-grafted polyethylene compatibilizer on the mechanical properties of the composite. When adding the compatibilizer, the tensile strength, toughness and strain at break were significantly improved. A deterioration of the mechanical properties was observed in the absence of compatibilizer. More recently, Melinte et al. [179] used photopolymerisation to prepare a hybrid nanocomposite of different types of photoinitiator-modified montmorillonites in polyurethane-dimethacrylate. The Young's modulus increased with montmorillonite content, but the transmittance decreased, especially for short visible wavelengths. Jlassi et al [95] used PGMA grafted bentonite in epoxy matrix to fabricate nanocomposites with enhanced storage modulus due to a better bound between clay and epoxy matrix. This nanocomposite shows better damping properties than neat epoxy or non-modified bentonite/epoxy nanocomposite. Even for composite filled with modified particles, often the improvement of some mechanical properties takes place to the detriment of other ones. For example Chandra et al. [56] treated alumina with low molecular weight poly(styrene-co-maleic anhydride) copolymer and compounded it with a PC matrix to prepare a transparent nanocomposite. At only 1 wt% of filler, this composite exhibited higher impact strength but no improvement of the ductility. Haase et al. [60] modified the surface of silica particles by grafting poly(styrene-co-acrylonitrile) copolymers chains before filling in PC matrix. Creep deformation and resistance against abrasive wear were greatly enhanced while strength and tensile modulus were moderately influenced by nanoparticle addition. It is known that it is difficult to simultaneously enhance the elastic modulus, the yield stress and the ductility of composite. Maillard et al. [180] accomplished this challenge with a composite made of PS matrix and silica particles grafted with PS. They claimed that this achievement was due to uniform nanoparticle spatial dispersion and strong interfacial binding between matrix and nanoparticles, thanks to the grafting of polymer chains with high M_n in comparison with the polymer of the matrix. Hu et al. [104] successfully enhanced the rigidity of a ZrO_2/PMMA transparent nanocomposite without loss of the toughness. In-situ bulk polymerization of methyl methacrylate/ZrO_2 was performed in the presence of a 2-hydroxyethyl methacrylate ligand. Hydrogen bonding interactions between the ligand and particles maintained ductile behavior while the rigidity was enhanced.

6.2. Thermal properties

The behavior of a material against temperature is a critical parameter determining its processing conditions, its final application and conditions of use (Table 6). The thermal stability of polymers can be improved by the addition of inorganic nanoparticles. Thermally stable transparent nanocomposites can be used in optics and electronics [44,83]. Wang et al. [135] increased the thermal stability of a transparent nanocomposite of PMMA filled with silica and zirconia nanoparticles. Through the addition of only 0.5 wt% of nanoparticles, the activation energy of the thermal decomposition of the PMMA main chains was raised from 69 to 99 $kJ.mol^{-1}$. The presence of the inorganic nanofillers in the composite reduced the movement of polymer chains and restrained the attack of free radicals on PMMA main chains. For various transparent nanocomposites such as clay/PMMA, [68,76,183] clay/ethylene-propylene-diene rubber [58], ZnO/PS [81], and TiO_2/PVA [79], the gain in thermal stability was ascribed to the addition of inorganic nanoparticles acting as heat insulators and exhibiting a barrier effect to oxygen and volatile degradation products. Signatures of improvement in the thermal stability of nanocomposites are for example the shift of the thermal degradation onset or the maximum degradation peak, and a slower degradation or a decrease of the thermal expansion coefficient. Sengupta et al. [122] dispersed silica nanoparticles in a polyamide matrix and obtained a transparent nanocomposite with improved thermal stability. The onset thermal degradation was 18 °C higher with the addition of only 0.8 wt% of silica nanoparticles. Hu et al. [104] incorporated up to 7 wt% of surface modified zirconia nanoparticles into PMMA matrix. The degradation of the resulting transparent nanocomposite was shifted to higher temperatures (as described in Fig. 3) and for a filler content of 7 wt% the peak of maximum degradation was increased to 57 °C.

Khanna and Singh [184] studied the degradation of a transparent CdS/PMMA nanocomposite. While the PMMA alone showed a sharp degradation, the addition of CdS nanoparticles clearly slowed the degradation. Liu et al. [110] varied the ZnO nanoparticles concentration up to 60 wt% in poly(butyl methacrylate) and studied the influence on the thermal expansion coefficient. Due to very small dimension of nanoparticles (4–6 nm) and an excellent dispersion in the matrix (nanoparticles were covalently attached to the matrix), the nancomposite kept its transparency even at very high loading. In comparison to pure poly(butyl methacrylate), the coefficient of thermal expansion of the obtained nanocomposite decreased from 325 to 193

UNCORRECTED PROOF

10^{-6}. K^{-1} below the glass temperature transition (T_g) and drastically decreased from 5378 to 1378 ppm K^{-1} above the T_g. A decrease of the thermal expansion coefficient was also reported for transparent nanocomposites made of silica dispersed into epoxy [94] silicone [94] and polyimide [131] matrices and for montmorillonite in polyimide [77]. The thermal stability of the nanocomposites was increased with a decrease of the thermal expansion and it also influenced in a positive way the mechanical properties. The dispersion state of the particles in the matrix, the matrix/filler interactions and the composite preparation method, have an important influence on the thermal stability of composite. Zhang et al. [161] fabricated a transparent ZnO/PMMA nanocomposite by in-situ particle formation and compared the thermal stability of the obtained composite to a composite formed by direct physical blending. The composite obtained by in-situ particle formation (which had strong interfacial interactions between the matrix and the fillers) exhibited a better thermal stability. Similarly, Demir et al. [185] increased the thermal stability of a transparent nanocomposite realized by in situ polymerization of ZnO nanoparticles in methyl methacrylate, while no significant improvements were obtained for a nanocomposite developed by direct physical blending. The glass transition temperature has been reported to increase with the filler content in several studies of transparent composites with high thermal stability [58,61,76,112,131]. The increase in Tg of the nanocomposites was due to strong matrix/filler interactions. However, few studies reported improvements of the thermal stability of composites when adding inorganic nanoparticles, while no significant changes occurred with the Tg due to weak matrix/fillers interactions [68,81]. The addition of inorganic nanoparticles into polymers can also enhance the fire behavior and the flame-retardant properties. Kim and Wilkie [183] added nanoclay and triphenyl phosphate into a transparent PMMA matrix and studied the fire properties of the transparent composite by cone-calorimetry. The addition of inorganic nanoparticles induced a decrease of the peak heat release rate and an increase in the average specific extinction area (related to the smoke production), indicating enhanced flame retardancy of the composite. Wang et al. [76] fabricated a transparent and flame-retardant modified clay/PMMA nanocomposite. The limiting oxygen index of the pure PMMA was increased by four units with the filler content of 5 wt%. Vahabi et al. [48] prepared a transparent PC filled with polyhedral oligomeric silsesquioxane and resorcinol bis(diphenylphosphate). The flammability, the smoke production and the heat released were reduced. These improvements in the nanocomposite fire behavior were ascribed to the formation of a cohesive char layer due to a condensed phase mechanism.

6.3. Transparent nanocomposites with barrier properties

The barrier properties of inorganic nanoparticles dispersed in polymers have been used to enhance the thermal properties of transparent nanocomposites (Table 7) but also to decrease the gas permeability of transparent composites used in food packaging, flexible electronics and pharmaceutical packaging [59,72,73,190]. Clay is the filler most used to decrease the oxygen permeability of composites. Priolo et al. [190] applied a layer-by-layer technique to realize a transparent clay/poly(ethylenimine) nanocomposite with high oxygen barrier properties. The layer-by-layer technique facilitated a high level of exfoliation and an orientation of the clay nanoplatelets. The transparent nanocomposite exhibited a brick wall nanostructure that essentially cut the oxygen permeability. Niknezhad and Isayev [73] strongly reduced the oxygen permeability of linear low density polyethylene (LLDPE) by adding 10 wt % of exfoliated nanoclays. The reduction of gas permeability of the transparent nanocomposites was ascribed to crystallinity of the polymer matrix and the presence of nanoclays making a more tortuous path for the oxygen diffusion. Similarly, Hong and Rhim [72] increased the oxygen barrier properties of clay/LLDPE nanocomposites. As the clay was not totally intercalated or exfoliated, the transparency of the composites decreased in comparison with the neat LLDPE. The nanocomposite also exhibited antimicrobial activity, which could be very interesting in food packaging applications to extend the shelf life by preventing microbial spoilage and proliferation. Durmus et al. [59] studied the effect of compatibilizers on the oxygen permeability of a transparent clay/PE nanocomposite. Whereas when adding a compatibilizer the nanocomposite showed high oxygen barrier properties, the gas permeation properties of the composite deteriorated without compatibilizer. De Melo et al. [71] achieved a biodegradable transparent nanocomposite composed of clay and a xanthan-starch matrix. With the incorporation of 2.5 wt% of nanoclays, the water vapor permeability and the water sorption capacity of the composite were reduced. Few studies used inorganic nanoparticles in transparent composites for their bacterial barrier properties. A transparent silver/PMMA nanocomposite with antibacterial properties was described by Akhavan et al. [160]. The nanocomposite was antibacterial against gram-negative bacteria. Such composites can be used for medical applications. Li et al. [173] obtained a transparent ZnO/PU nanocomposite with strong antibacterial activity. The antibacterial efficiency (especially against Escherichia coli) increased with the content of ZnO nanoparticles in the composite (up to 4 wt%). The antibacterial activity of the nanocomposite was due to the formation of hydrogen peroxide from the surface of ZnO nanoparticles. In the same way, Youssef et al. [191] described two types of nanocomposites of chitosan/polyethylene Glycol/ Calcium silicate with either ZnO NPs or tartazyne dye (E102). Both showed antibacterial properties but as expected, the composite with the dye was more transparent than the composite with the ZnO NPs due to the scattering of light by the particles. Nkeuwa et al. [192] studied the Water Vapor Transmission Rate (WVTR) in acrylate/cloisite nanocomposite coatings for wood. For only 1 wt.% of cloisite, the WVTR was reduced by 25% and 40% according to the type of cloisite, with a transmittance value measured at 80–86%. The decrease of the WVTR is explained by a more tortuous path due to the presence of the cloisites. In the same way, Kang et al. [193] fabricated a silica-epoxy nanocomposite capable of reducing the WVTR from 4 $g.m^{-2}.day^{-1}$ (for neat epoxy matrix) to 1.5 $g.m^{-2}.day^{-1}$ for the nanocomposite with 30 wt. % of silica nanoparticles while maintaining a high transmittance value (90%). Two papers deal with α-ZrP nanoparticles incorporated in an epoxy matrix. Wong et al. [194] showed that their nanocomposite decreased the Oxygen Transmission Rate by 80% and the permeability by 96% at 0% RH. At higher RH rates, the decrease is lower but remains significant. They included some photographs of their composite showing some transparency in spite of a brown coloration. Kim et al. [195] described a nanocomposite that allowed thereduction of the WVTR by 92% without affecting the transmission of the light.

6.4. Transparent nanocomposites with magnetic properties

Magnetic nanocomposites can be obtained by the addition of metal nanoparticles or iron oxide (Fe_2O_3, Fe_3O_4 or ferrite) nanoparticles into a polymer matrix (Table 8). These kind of nano composites can find potential applications in purification and concentration of proteins, contrast agents in imaging, mediators in hyperthermia, carriers for guided drug delivery, information storage, bioprocessing and magnetic refrigeration [141,199]. Unfortunately, most of the magnetic materials are not transparent in the visible domain [141], conse-

UNCORRECTED PROOF

quently very few studies have been reported on transparent nanocomposites with magnetic properties. Ziolo et al. [141] realized a magnetic, transparent nanocomposite by filling a sulfonated polystyrene matrix with (5–10 nm) γ- Fe_2O_3 nanoparticles. The nanocomposite with filler content of 21.8 wt% had a magnetic saturation moment of 15 emu.g^{-1}, at room temperature. The composite did not exhibit any hysteresis which typically represented the behavior of a superparamagnetic material. Li et al. [106] achieved 5 mm thick transparent nanocomposite with superparamagnetic properties. In a first step 10 nm iron oxide nanoparticles were capped with oleic acid and then in-situ polymerization in methyl methacrylate was performed. The saturation magnetization was increased from 0.0025 to 0.015 emu.g^{-1} when the filler content rose from 0.08 to 0.2 wt%. The very small dimension of the nanoparticles, their good dispersion in the matrix and the low content of filler promoted transparency of the nanocomposites, even for thick samples.

6.5. Optical properties

The use of inorganic particles for optical properties might be one of their first known applications. For example, gold nanoparticles have been used to color glass for centuries. Over the two last decades, interest has increased in the design of transparent inorganic/polymer nanocomposites with specific optical properties such as light absorption (UV, infrared, visible), extreme refractive indices, photoluminescence, dichroism or non-linear optical properties. The optical properties of transparent nanocomposites are governed by the nature, size and spatial distribution of the inorganic particles. Intrinsic optical properties such as refractive index, color absorption and color emission depend on the inorganic particle size. Particles with a diameter smaller than 10 nm (D < 10 nm) undergo quantum confinement effects, resulting in different optical properties than the corresponding bulk inorganic material [1,2,6]. The spatial distribution of the inorganic nanoparticles also plays a major role. Indeed, a random distribution of individually dispersed nanoparticles promotes optical transparency, photoluminescence, UV and IR absorption while an ordered distribution may favor iridescence and an uniaxially oriented distribution of particles may produce dichroism [2,202].

6.5.1. Ultra-violet (UV) absorption properties

In recent years with the modification of the atmospheric composition and the thinning of the ozone layer, interest in UV-protective materials has increased. A large variety of organic UV-absorbers exists but they lack long-term stability. On the other hand inorganic UV-absorbers exhibit higher photo-stability and become of major interest when incorporated in polymers. UV-shielding transparent nanocomposites can be achieved by filling transparent polymers with particles absorbing light in the UV region without absorbing in the visible domain and with particle dimension small enough to strongly reduce visible light scattering (Table 9). Promising candidates for these kinds of applications are oxide semiconductors such as ZnO, TiO2 and CeO2 with band-gap energies around 3 eV [1]. With these kinds of nanoparticles, the UV-filtering is due to two phenomena: UV light absorption and UV light scattering [203]. Oxide semiconductors absorb UV light by means of their electronic structures through interband absorption mechanism. The energy of the UV photon is absorbed and induces an electron transfer between the valence band and the conduction band. For particles having smaller dimensions compared to the wavelength ($D/\lambda \ll 1$), the light scattering by particle is described by the Rayleigh theory (see section A-II-1). The intensity of the Rayleigh scattered light is inversely proportional to the wavelength to the fourth power ($I \propto \frac{1}{\lambda^4}$), i.e. the UV light ($10 < \lambda < 400$ nm) is scattered more efficiently than the visible light ($400 < \lambda < 800$ nm). On the basis of previous studies concerning transparent composites with UV shielding properties, it was concluded that the dispersion of the nanoparticles is a key point to produce efficient materials. To fulfill this condition, the particle surface is often modified. Many previous studies that have reported on transparent nanocomposites with UV shielding properties were performed on thin polymer films with typical thickness of 1–100 μm with inorganic particles loading of 1–10 wt%. Several examples of such composites were prepared from different inorganic nanoparticles and polymer matrices: unmodified or modified ZnO nanoparticles in PMMA [161,185,204,205]; PS [81]; poly(vinyl alcohol) (PVA) [206]; poly(butyl acrylate) [110]; polyethylene and polypropylene [207]; copolymers of polyethylene and PVA [146]; TiO2 nanoparticles in PMMA [61]; PVA [79,208]; PS and PC [209]; Chitosan [210]; CeO2 nanoparticles in PS [37] and castor oil resin [211]; FeS2 nanoparticles in PVA and poly(vinyl pyrrolidone) [145]; alumina nanowhiskers in PC [111] or modified ITO in PUA [87]. Although the values of refractive indices of the matrix and fillers were different in those composites, the transparency was acceptable due to the low film thickness, the small size and the good dispersion state of the nanoparticles. In some cases, a loss of transparency was observed due to light scattering when the size of the particle [90] and the filler content [208] were increased (Fig. 4).

Parlak and Demir [37] achieved the fabrication of a composite which efficiently absorbed UV wavelengths while maintaining a high transparency in the visible domain. PMMA chains were grafted onto the surface of CeO_2 nanoparticles to match the refractive index of the nanoparticles with that of a PS matrix. Several studies described the improvement of the UV shielding properties of transparent nanocomposites with only low amounts of nanoparticles. Sun et al. [212] and Li et al. [90] obtained high UV shielding by adding 0.8 wt% of ZnO nanoparticles in PMMA and 0.07 wt% in epoxy matrix, respectively. Godnjavec et al. [213] filled a polyacrylic matrix with only 0.6 wt% of TiO_2 nanoparticles and observed good UV shielding. Matsuno et al. [178] achieved high UV absorption with TiO_2 content less than 1 wt% in PS matrix. They also studied the influence of surface modification of TiO_2 nanoparticles on the UV filtering properties and found that when grafting PS chains onto the TiO_2 surface the UV absorption was ten times increased compared to unmodified particles. Few research works combined low filler content and very small particle dimensions to obtain thicker transparent composites (1–4 mm) capable of filtering UV rays [84,91,102]. The thicker transparent nanocomposite was achieved by Li et al. [214] via in situ sol-gel polymerization of a ZnO/methyl methacrylate dispersion in the presence of a coupling agent. It resulted in a transparent nanocomposite of PMMA filled with highly dispersed 5 nm ZnO nanoparticles. The 1 cm thick nanocomposite exhibited strong UV absorption at a filler content of only 0.017 wt%. The size of the particles plays an important role in the UV absorption of composites. The decrease in the particle size induces a blue shift of the UV absorption edge. For example, Xiong et al. [215] studied the UV absorption properties of a transparent PS-PnBA copolymer matrix filled with ZnO particles of different diameters 60 nm, 100 nm and 1 μm. The decrease of the particle diameter led to a blue shift of the UV absorption edge. More interestingly, for semiconductor particles with dimensions below 10 nm, quantum confinement effects increase the band gap energy and cause a blue shift of the absorption edge compared to the bulk semiconductor materials. Jeeju et al. [216] studied the UV absorption as a function of ZnO particle size in a transparent PS matrix. The ZnO size varied from 5 to 35 nm. For particles less than 10 nm they observed a band gap enlargement from 3.2 to 4.15 eV and a blue shift of the adsorption edge in comparison to 35 nm particles.

UNCORRECTED PROOF

6.5.2. Infra-red (IR) filtering properties

IR absorbing and reflecting nanocomposites can be of great interest for energy saving windows in buildings, automobiles, heat mirrors, heat insulating coatings, contact lenses and anti-reflecting optical filters. The most encouraging IR absorbing particles are indium tin oxide (ITO) and antimony tin oxide (ATO) particles. This kind of n-type semiconductor particle can absorb IR radiation by free carrier absorption. The absorption of an IR photon induces the movement of a conduction electron in a higher energy state within the conduction band. ITO and ATO particles are also able to filter UV light by interband absorption but unlike TiO_2, ZnO, and CeO_2 particles, the UV adsorption edge is not sharp [222]. The literature concerning the field of IR absorption is dominated by patents and little scientific documentation is available. However, some studies have been reported on IR filtering transparent nanocomposites. Zhang et al. [223] fabricated a 60 μm thick transparent nanocomposite made of a PMMA-PnBA copolymer matrix filled with ATO nanoparticles. The nanocomposite transmittance in the near IR range (800–2600 nm) decreased strongly when increasing the ATO nanoparticles content from 3 to 10 wt%, while it was transparent in the visible domain. Liu et al. [224] realized a 30 μm transparent nanocomposite of ITO/ acrylic polyurethane which filters 50% of the IR rays at 1500 nm and 45% of the UV rays at 350 nm at ITO loading of 5 wt%. Tao et al. [222] filled an epoxy matrix with poly(glycidyl methacrylate) grafted ITO nanoparticles. The miscibility of the grafted chains with matrix chains promoted a high dispersion of the nanoparticles and so a high transparency in the visible domain was obtained. The 20 μm thick nanocomposite was filled with 5, 10, 20, 35 and 60 wt% of ITO particles. As the IR shielding efficiency depends on the free carrier concentration, the nanocomposite exhibited better IR shielding at high ITO contents (60 wt%) and almost 100% of the IR was filtered. The increase of the ITO concentration shifted the IR transmission cut-off wavelength toward a shorter wavelength. The UV absorption also increased with the increase of ITO concentration. Nevertheless, the transmittance of visible light decreased at high loadings. The UV–vis and near IR transmittance spectra are presented in (Fig. 5).

Luo et al. [88] dispersed Al-doped ZnO nanoparticles in epoxy matrix. At 0.08 wt% of fillers, the nanocomposite exhibited IR shielding, strong UV absorption while keeping its transparency in the visible domain. Mandzy and Grulke [225] achieved an IR mirror thin film made of fifteen discrete layers of alternated low (SiO_2/polyacrylate) and high (TiO_2/polyacrylate) refractive index layers. The final nanocomposite film, with a thickness of 2.4 μm, kept its transparency in the visible domain and reflected 90% of the IR radiation at 1064 nm. More recently, Ireni et al. [226] prepared nanocomposites of Poly(thiourethane-urethane)-urea with titania modified by sulfur-rich hyperbranched polyols. The nanocomposite is presented as transparent, even with a rather high titania loading (up to 5 wt.%), and reflects more than 90% of the NIR wavelengths (Table 10).

6.5.3. Coloration properties

Gold nanoparticles have been used for centuries to color glass. Indeed, some metal inorganic particles absorb specific parts of the visible light and therefore provide an intense coloration. These inorganic nanoparticles were filled inside a polymer matrix to provide transparent nanocomposite films with specific color properties provided by the particles (Table 11). The color of those metal particles depends on the particle size and also on the distance between particles. Heffels et al. [227] filled a poly(vinyl alcohol) matrix with gold nanoparticles of 9.5, 43 and 49 nm, this resulted in the coloration of the nanocomposite respectively in red, purple and blue. Carotenuto [228] achieved a heavily red colored transparent nanocomposite (Fig. 6). By loading 8 wt% of silver nanoparticles into a poly(vinylpyrrolidone) (PVP) matrix, the nanocomposite kept its transparency while it strongly absorbed the light at a wavelength of 410 nm.

Carotenuto and Nicolais [229] obtained a purple-colored transparent nanocomposite by filling a PS matrix with 10 nm PVP modified gold nanoparticles. Biswas et al. [230] observed a red shift of the maximum absorption of Teflon loaded with silver particles when the size of particles was increased. The color of the transparent composite changed from yellow to golden brown yellow. The color of metal particles can also be tuned by changing the inter-particle distance. Kirchner and Zsigmondy [231] dispersed silver and gold particles in gelatin and used the swelling properties of the gelatin to change the inter-particle distances. The composite could reversibly change its color through drying or swelling the composite with water. The maximum absorption shifted to higher wavelength when inter-particle distances were reduced. Liou et al. [114] used silver nanowires (AgNW)/PDMS electrodes with Heptyl Viologen to form a new electrochromic device that changes its aspect from colorless to blue. To circumvent the issue of achieving high transparency without significant loss of conductivity due to the low attractive force between AgNWs and PDMS, the AgNWs were casted onto a hydrophobic Teflon plate as the weak attractive force with Teflon favoring their embedding with PDMS viscous liquid [114].

6.5.4. Extreme refractive indices

Composite with extreme refractive indices (ultrahigh $n > 2$ or ultralow $n < 1$) can find applications in optical filters, lenses, optical waveguides, reflectors, optical adhesives, solar cells and anti-reflections films [1,2,6,7]. Inorganic materials exhibit a wide range of refractive indices from values below 1 (e.g., gold) to values above 3 (e.g., lead sulfide PbS). Since most polymers exhibit refractive indices between 1.3 and 1.7, the incorporation of inorganic particles into polymeric matrices is a way to tune the refractive index of the composites and to obtain composites with extreme refractive indices (Table 12). The preparation of transparent composite with extreme refractive index is a subtle challenge because the consistent difference in refractive index between the matrix and fillers is the major reason for opacity in composites. To suppress light scattering by the particles and loss of transparency of the composite, particles with dimensions well below the considered wavelength ($D/\lambda << 1$) and an optimal dispersion of particles in the matrix are required. Inorganic particles with such dimensions exhibit different refractive indices than the analog bulk materials. For example, Kyprianidou-Leodidou et al. [233] showed that the refractive index of PbS particle was size dependent by observing a decrease of the refractive index value for particles smaller than 25 nm.

Most studies on transparent composites with high refractive indices have been performed with thin composite films (< 100 μm), with inorganic nanoparticles having diameters around 10 nm. Such transparent nanocomposites were obtained with various polymer matrices and inorganic nanoparticle fillers, including: PbS in poly(thiourethane) [238]; TiO_2 in any of several matrices: epoxy [98,235,236], PVA [208], polyimide [237,238], a styrene and maleic anhydride copolymer [236] or PMMA [239]; ZnS or ZnO in poly(urethane-methacrylate) [99] and caprylic capric triglyceride, respectively [240]; TiO_2 or ZrO_2 nanoparticles in polyimides [238,241] or polyimidoethers [242].

The nanocomposite refractive index could be tuned by increases of up to 0.4 for these systems. Nevertheless, some of these composites showed a significant decrease of transparency when the filler content was increased (up to ≈ 30–40 wt%) [98,208,229,231]. Zim-

UNCORRECTED PROOF

mermann et al. [243] reported a transparent composite with the highest refractive index (n = 2.4). For that purpose, they synthesized in-situ well-dispersed PbS nanoparticles of 5–20 nm in a gelatin solution. This solution was then spin-coated to obtain transparent thin films with a thickness of 40 nm-2 μm. The refractive index of the gelatin matrix initially equaled to 1.5 at 632.8 nm, but was raised to the value of 2.4 when 55 vol% of PbS nanoparticles were added. The transparency of the composites was not fully documented, but the authors claimed that the light passed through the films without being scattered as far as could be judged by the eye. As described in Fig. 7, the refractive index of the composite increased linearly with the volume fraction of PbS nanoparticles.

The linear evolution of the composite refractive index with the volume fraction of inorganic fillers has also been reported in several studies [83,208,234,237,244]. Few studies reported the fabrication of thicker (1–5 mm) transparent composites with high refractive indices [239,240,89,217]. The transparency could be kept by using well-dispersed nanoparticles with diameters of only 2–6 nm and without exceeding filler contents of 20 wt %. Zimmermann et al. [244] achieved gold/gelatin composites with a very low refractive index (n = 0.963). The refractive index of the composite decreased linearly from 1.537 to 0.963 at λ = 632.8 nm, respectively, when the weight fraction of gold nanoparticles increased from 0 to 48 wt-%. Although the transparency of the composites was not studied or mentioned in the article, as the gold nanoparticles had diameters of 2–10 nm and the thickness of the composite was 200–400 nm, it might be assumed that for low filler content the composite exhibited transparency.

To produce transparent, strong and flexible fluorinated polyimide (PI) nanocomposite with a low dielectric constant of 2.09 and high tensile strength of 300.1 MPa, the interfacial interaction between the PI matrix and two-dimensional fluorographene nanofillers (FG) was optimized by the grafting of 2,2′-bis(trifluoromethyl)-[1,1′-biphenyl]-4,4′-diamine molecule [182].

6.5.5. Photoluminescence

Under UV light excitation the II-VI semi-conductor nanocrystals exhibit photoluminescence properties. The emission colors of those particles can be tuned by varying the concentration or the particle size due to quantum confinement effects. The addition of dopants and defects can also change the emission colors of the semi-conductor particles [1]. Luminescence in the visible region is produced by those nanocrystals or quantum dots (for example ZnO nanoparticles with diameter ≤ 7 nm) [34]. Semi-conductor nanoparticles exhibit two usual types of emission: an excitonic and a trap emission. The excitonic emission is sharp and is located in the near absorption edge (UV region), while the trap emission is broad and emits a Stokes shift (i.e., an emission at longer wavelength than the absorbed wavelength due to energy loss) [184]. The incorporation of semi-conductor nanocrystals into polymer matrix allows for the preparation of nanocomposites which find application in lighting, screen, diode, photodetectors and display devices [1,2,7]. To avoid the deterioration of the semi-conductor photoluminescence, the nanocrystals often need a surface modification step before introduction into the polymer matrix. Various transparent nanocomposites with photoluminescent properties were reported (Table 13). Zhang et al. [100] filled a transparent PS matrix with surface modified cadmium telluride (CdTe) nanoparticles of different sizes. The resulting composites exhibited transparency and different color emissions depending on the size of the fillers. A green, yellow, orange and red luminescence was observed for composites filled with CdTe nanoparticles of 2.8, 3.3, 3.6 and 4.0 nm, respectively. Khanna and Singh [184] obtained a transparent composite from cadmium sulfide (CdS) nanoparticles dispersed in a PMMA matrix. The luminescence of the composite varied with the CdS concentration. At 2 wt% of CdS nanoparticles the composite emitted a blue or blue-green emission whereas at higher filler contents the composite emitted in the yellow-orange region. Heiba et al. [249] used CdS prepared at different temperatures in a PVA matrix to obtain a photoluminescent nanocomposite. In the visible region, the peak of photoluminescence corresponds to the green and the intensity of the peak is dependent on the temperature of preparation of the NPs of CdS. As the toxicity of the cadmium might be an issue regarding its use in commercial applications, ZnO and ZnS appear to be more suitable than the cadmium compounds for the fabrication of composites with photoluminescent properties [1]. Transparent composites with bright visible luminescence were achieved by adding either manganese doped ZnS nanoparticles into PMMA [250], or by introducing ZnO and modified ZnO nanoparticles into poly(butanediolmonoacrylate) [84], PMMA [161], and epoxy [92] matrices. Different sizes of ZnO quantum dots were embedded in silicone [34], PMMA [102] and poly(hydroxyethyl methacrylate) [101] matrices. The recovered composites were transparent and emitted tunable colors (from blue to orange). In each case the photoluminescence was blue-shifted when the particle size decreased. Some studies showed that the ZnO nanoparticles surface could be passivated to quench the emission of light in the visible domain and shift the complete emission towards the UV region. This phenomena was reported for different transparent composites with ZnO nanoparticles dispersed in PVA [206], PS [216], and PMMA [251,252]. The emission in the visible domain is due to defects (surface traps) and impurity-related states in ZnO, so the surface modification can quench this visible luminescence [216]. On the other hand, the emission in the UV domain originates in the radiative recombination of electrons from conduction band with hole from the valence band [161]. A blue shift of the UV photoluminescence was also reported when the size of the nanoparticles decreased [215,251]. Tan et al. [25] achieved the fabrication of a transparent composite with bright IR-emitting properties. Cerium fluoride nanoparticles were doped with erbium and ytterbium (CeF_3:Yb-Er) and incorporated into a PS matrix. Upon excitation at λ = 975 nm the composite exhibited a strong emission around λ = 1530 nm. Such composites can find applications in optical amplifiers, waveguides, laser materials and implantable medical devices.

6.5.6. Transparent nanocomposites with dichroism properties or nonlinear properties

Uniaxially oriented distribution of metal particles into polymer matrices can result in dichroic composites. This kind of composite exhibits different colors when they are illuminated by polarized light. The absorption of the visible light and the color of the composite change depending on the angle between the orientation direction of the metal particles in the composite and the polarization plane of the incident light [6,258]. To align the particles into the polymer matrix different techniques were developed such as solid-state drawing or melt elongation [2,6]. The melt elongation consists of stretching the composite at melt-state and produces dichroic composites with more reproducibility than the solid-state drawing [258]. Recently, melt elongation was used to obtain dichroic composites made of gold nanoparticles and nanorods dispersed in PVA [259,260] and PE [258] transparent matrices. The color of these composites changed at parallel or perpendicular direction between the stretch direction of the composites and the polarization plane of the light. Dichroic composites might be used as optical filters and liquid- crystal displays [258]. Over the past decade, interest in the study of the nonlinear optical properties of polymer nanocomposites has grown. Such nanocomposites are of interest for applications in high-speed communications net-

UNCORRECTED PROOF

works, including all-optical switching, wavelength manipulation, signal processing devices, optical computing, real time holography, optical correlates and phase conjugators [147]. Under very high light intensities typically provided by lasers, some inorganic particles such as semiconductor nanoparticles exhibit nonlinear optical properties. Investigations of different transparent composites with nonlinear optical properties have been reported. Du et al. [147] studied the optical properties of a PS matrix filled with CdS nanoparticles. The transparent composite showed 3rd order and possible higher order nonlinearity, and the nonlinear refractive index of the composites varied with the input laser energy and with the CdS nanoparticle concentration. Nonlinearity of ZnO nanoparticles in PMMA was studied by Kulyk et al. [261]. The transparent composite presented 2nd and 3rd order nonlinear susceptibilities higher than the ones of bulk ZnO. Asunskis et al. [144] incorporated PbS nanoparticles into PE, PS, poly(1-butene) and poly(1-decene) matrices. The four composites obtained were transparent and exhibited a strong nonlinear absorption due to several mechanisms such as free carrier absorption, trapped-state absorption and multiphoton absorption. Ultrafast nonlinear optical properties of TiO_2 nanoparticles embedded in PMMA were reported by Elim et al. [262]. A third order optical nonlinearity was observed with a short recovery time of only $\approx$ 1.5 ps. The influence of TiO_2 crystallinity in PMMA on the nonlinear optical properties was studied by Yuwono et al. [263,264]. The transparent composite filled with the TiO_2 nanoparticles of higher crystallinity exposed enhancement in the 3rd order susceptibility, nonlinear refractive index and nonlinear absorption (two-photon absorption) (Table 14).

7. Conclusion and perspectives

This literature review was focused on transparent nanocomposites based on polymer matrices filled with inorganic nanoparticles, showing that a wide range of transparent nanocomposites has been fabricated with various types of thermoplastic and thermoset transparent matrices. Depending on the desired final properties (mechanical, thermal, optical…), those matrices can be filled with different kinds of inorganic fillers such as metal and metal alloys, metal oxides, semiconductors and minerals. In the evolution of the particles included in the nanocomposite clays used to improve the mechanical properties of the polymers have been followed by the use of rare earths for semi-conductors. Several techniques were reported to fabricate transparent nanocomposites. Each one has its own advantages and drawbacks. In-situ formation of both matrix and particles is an interesting one-step process that provides composites filled with well dispersed particles. However, a disadvantage might be a lack of control over the particle size. Direct blending (in melt or solvent) is an easy process convenient for large-scale production but it often requires a prior surface modification step. The incorporation of inorganic particles into a polymer matrix modifies the transparency of the composite. The light scattered by particles is mainly responsible for the transparency loss. The size of the particles, or aggregates of particles, and the difference of refractive indices between the matrix and the fillers, are the two major parameters that govern the phenomena of light scattering by the composite. Different strategies have been developed to minimize the light scattered by the particle to achieve an optimal transparency of the composite. The most widely used strategy is to strongly decrease the size of the particles used as fillers. This approach requires a good control of the particle size and an optimal dispersion of the particles into the matrix. As the inorganic nanoparticles easily tend to aggregate, a surface modification step of the nanoparticles with organic compounds is often necessary to promote the dispersion of particles into the matrix. However, few studies reported a different approach to maintain the composite transparency by matching the refractive indices of the matrix and the fillers. The design of hybrid core@shell nanoparticles based on an inorganic core and a polymer shell appeared to be a promising approach to control both the particle dispersion into the matrix and to tune the average refractive index of the core@shell particle. The evaluation of transparency, especially when it is a required property should be more complete, e.g., in addition to a numerical transparency, the data should include the specimen shape and thickness, the nanoparticle content should be systemically indicated. Measurements should always be carried out as photographs limit effective evaluation. Characterizing the angular distribution of the transmitted light could be of interest to provide a more precise overview of how the transparency could be perceived by the eye.

Acknowledgements

Communauté d'Agglomération Pau Béarn Pyrénées (CAPBP), IMT Mines Ales, CNRS and University Pau & Pays Adour are gratefully acknowledged for their financial support.

References

[1] H. Althues, J. Henle, S. Kaskel, Functional inorganic nanofillers for transparent polymers, Chem Soc Rev 36 (2007) 1454–1465.
[2] S. Li, M.M. Lin, M.S. Toprak, D.K. Kim, M. Muhammed, Nanocomposites of polymer and inorganic nanoparticles for optical and magnetic applications, Nano Rev 1 (2010), 5214/1-19.
[3] S. Mallakpour, V. Behranvand, Nanocomposites based on biosafe nano ZnO and different polymeric matrixes for antibacterial, optical, thermal and mechanical applications, Eur Polym J 84 (2016) 377–403.
[4] I.L. Ngo, S. Jeon, C. Byon, Thermal conductivity of transparent and flexible polymers containing fillers: a literature review, Int J Heat Mass Transf 98 (2016) 219–226.
[5] B. Faure, G. Salazar-Alvarez, A. Ahniyaz, I. Villaluenga, G. Berriozabal, Y.R. De Miguel, et al., Dispersion and surface functionalization of oxide nanoparticles for transparent photocatalytic and UV-protecting coatings and sunscreens, Sci Technol Adv Mater 14 (2013), 023001/1-23.
[6] W. Caseri, Inorganic nanoparticles As optically effective additives for polymers, Chem Eng Commun 196 (2008) 549–572.
[7] S. Kango, S. Kalia, A. Celli, J. Njuguna, Y. Habibi, R. Kumar, Surface modification of inorganic nanoparticles for development of organic–inorganic nanocomposites–a review, Prog Polym Sci 38 (2013) 1232–1261.
[8] B.M. Novak, Hybrid nanocomposite materials - between inorganic glasses and organic polymers, Adv Mater 5 (1993) 422–433.
[9] G. Kickelbick, Concepts for the incorporation of inorganic building blocks into organic polymers on a nanoscale, Prog Polym Sci 28 (2003) 83–114.
[10] F. Yan, J. Texter, Capturing nanoscopic length scales and structures by polymerization in microemulsions, Soft Matter 2 (2006) 109–118.
[11] L.L. Beecroft, C.K. Ober, Nanocomposite materials for optical applications, Chem Mater 9 (1997) 1302–1317.
[12] S.K. Kumar, N. Jouault, B. Benicewicz, T. Neely, Nanocomposites with polymer grafted nanoparticles, Macromolecules 46 (2013) 3199–3214.
[13] M. Kotal, A.K. Bhowmick, Polymer Nanocomposites from modified clays: recent advances and challenges, Prog Polym Sci 51 (2015) 127–187.
[14] A. Christmann, C. Longuet, J.M. Lopez-Cuesta, Tansparent polymer nanocomposites: a new class of functional materials, in: J. Tadakoum (Ed.), Nanomaterials and surface engineering, John Wiley & Sons Inc, Hoboken, 2010, pp. 31–52.
[15] C.L. Tsai, H.J. Yen, G.S. Liou, Highly transparent polyimide hybrids for optoelectronic applications, React Funct Polym 108 (2016) 2–30.
[16] G. Mie, Beiträge zur Optik trüber Medien, speziell kolloidaler Metallösungen, Ann Phys 330 (1908) 377–445.
[17] H.C. Van De Hulst, Light scattering by small particles, John Wiley & Sons Inc, New-York, 1957, 470 pp.
[18] C.F. Bohren, D.R. Huffman, Absorption and scattering of light by small particles, John Wiley & Sons Inc, New York, 1988, 547 pp.
[19] M. Kerker, The scattering of light and other electromagnetic radiation, John Wiley and Sons Inc, New York, 1969, 688 pp.
[20] J.A. Stratton, Electromagnetic theory, McGraw-Hill, New York, 1941, 520 pp.

UNCORRECTED PROOF

[21] R.J. Nussbaumer, Synthese und Charakterisierung von Rutilnanopartikeln und deren Einbau in transparente Polymer-Nanoverbundwerkstoffe. DScTech Thesis, Eidgenössischen Technischen Hochschule Zürich, Zürich, 2004, 190 pp.
[22] H. Lin, D.E. Day, J.O. Stoffer, Optical an mechanical properties of optically transparent poly(methyl methacrylate) composites, Polym Eng Sci (1992) 344–350.
[23] Hsieh A.J. Yu JH, G.C. Rutledge, Novel transparent PMMA composites for optical tagging, Army research laboratory report ARL-TR-5354, 2010, 18 pp.
[24] T.C. Gilmer, P.K. Hall, H. Ehrenfeld, K. Wilson, T. Bivens, D. Clay, et al., Synthesis, characterization, and mechanical properties of PMMA/Poly(aromatic/aliphatic siloxane) semi-interpenetrating polymer networks, J Polym Sci Part A: Polym Chem 34 (1996) 1025–1037.
[25] M.C. Tan, S.D. Patil, R.E. Riman, Transparent infrared-emitting CeF3:Yb-Er polymer nanocomposites for optical applications, ACS Appl Mater Interfaces 2 (2010) 1884–1891.
[26] L. Bombalski, H. Dong, J. Listak, K. Matyjaszewsk, M.R. Bockstaller, Null-scattering hybrid particles using controlled radical polymerization, Adv Mater 19 (2007) 4486–4490.
[27] J.C.M. Garnett, Colours in metal glasses and in metallic films, Phil Trans R Soc London A (1904) 38–420.
[28] J.C.M. Garnett, Colours in metal glasses, in metallic films, and in metallic solutions. II, Phil Trans R Soc London A (1906) 237–288.
[29] J.M. Lamarre, Propriétés optiques linéaires et non-linéaires de nanocomposites métal/diélectrique anisotropes. PhD Thesis, Université Paul Cézanne - Aix-Marseille, Marseille FR, 2008, 240 pp.
[30] Y.Q. Li, S.Y. Fu, Y. Yang, Y.W. Mai, Facile synthesis of highly transparent polymer nanocomposites by introduction of core–Shell structured nanoparticles, Chem Mater (2008) 2637–2643.
[31] A. Christmann, Elaboration et propriétés de nanocomposites transparents à matrice polycarbonate. PhD Thesis, Université de Montpellier II, Montpellier FR, 2007, 214 pp.
[32] H. Suzuki, M. Taira, K. Wakasa, M. Yamaki, Refractive-index-Adjustable fillers for visible-light-Cured dental resin composites - preparation of TIO2-SIO2 glass powder by the sol-gel process, J Dent Res 70 (1991) 883–888.
[33] Y. Li, Y. Yang, C.Q. Sun, S. Fu, Significant enhancements in the fluorescence and phosphorescence of ZnO quantum Dots/SiO2 nanocomposites by calcination, J Phys Chem C 112 (2008) 17397–17401.
[34] Y. Yang, Y.Q. Li, H.Q. Shi, W.N. Li, H.M. Xiao, L.P. Zhu, et al., Fabrication and characterization of transparent ZnO–SiO2/silicone nanocomposites with tunable emission colors, Composites Part B 42 (2011) 2105–2110.
[35] H. Schulz, L. Mädler, S.E. Pratsinis, P. Burtscher, N. Moszner, Transparent nanocomposites of Radiopaque, flame-made Ta2O5/SiO2 particles in an acrylic matrix, Adv Funct Mater 15 (2005) 830–837.
[36] L. Mädler, F. Krumeich, P. Burtscher, N. Moszner, Visibly transparent & radiopaque inorganic organic composites from flame-made mixed-oxide fillers, J Nanopart Res 8 (2006) 323–333.
[37] O. Parlak, M.M. Demir, Toward transparent nanocomposites based on polystyrene matrix and PMMA-grafted CeO2 nanoparticles, ACS Appl Mater Interfaces 3 (2011) 4306–4314.
[38] K. Matsukawa, T. Fukuda, S. Watase, H. Goda, Preparation of photo-curable thiol-ene hybrids and their application for optical materials, J Photopolym Sci Technol 23 (2010) 115–119.
[39] D.J. Krug, M.Z. Asuncion, V. Popova, R.M. Laine, Transparent fiber glass reinforced composites, Compos Sci Technol 77 (2013) 95–100.
[40] S. Shin, B.C. Kim, E. Chang, J.K. Cho, D.H. Suh, A biobased photocurable binder for composites with transparency and thermal stability from biomass-derived isosorbide, RSC Adv 4 (2014) 6226–6231.
[41] D.F. Cheng, A. Hozumi, Highly loaded silicone nanocomposite exhibiting quick thermoresponsive optical behavior, ACS Appl Mater Interfaces 3 (2011) 2219–2223.
[42] D.J.O. Brien, J. Robinette, J.R. Heflin, J. Ridley, Nanocomposite interphases for improved transparent polymer composite materials, Army research laboratory report ARL - TR-4527, 2008, 32 pp.
[43] H. Zou, S. Wu, J. Shen, Polymer/silica nanocomposites: preparation, characterization, properties, and applications, Chem Rev 108 (2008) 3893–3957.
[44] Anonymous, ASTM E284, standard terminology of appearance, ASTM International, West Conshohocken PA, 2017, 25 pp.
[45] Anonymous, ASTM D1746 standard test method for transparency of plastic sheeting, ASTM International, West Conshohocken PA, 2015, 4 pp.
[46] Anonymous, ASTM D1003 standard test method for haze and luminous transmittance of transparent plastic, ASTM International, West Conshohocken PA, 2013, 7 pp.
[47] R. Zhou, T. Burkhart, Optical properties of particle-filled polycarbonate, polystyrene, and poly (methyl methacrylate) composites, J Appl Polym Sci 115 (2009) 1866–1872.
[48] H. Vahabi, O. Eterradossi, L. Ferry, C. Longuet, R. Sonnier, J.M. Lopez-Cuesta, Polycarbonate nanocomposite with improved fire behavior, physical and psychophysical transparency, Eur Polym J 49 (2013) 319–327.
[49] Z.W. Wilchinsky, Clarity measurement of polymer films, J Appl Polym Sci 5 (1961) 48–52.
[50] A. Krell, T. Hutzler, J. Klimke, Transmission physics and consequences for materials selection, manufacturing, and applications, J Eur Ceram Soc 29 (2008) 207–221.
[51] F. Metelli, The perception of transparency, Sci Am 230 (1974) 90–98.
[52] E.H. Adelson, Lightness perception and lightness illusions, New Cogn Neurosci 3 (2000) 339–351.
[53] B.L. Anderson, A theory of illusory lightness and transparency in monocular and binocular images: the role of contour junctions, Perception 26 (1997) 419–453.
[54] A. Kitaoka, A new explanation of perceptual transparency connecting the X-junction contrast-polarity model with the luminance-based arithmetic model, Jpn Psychol Res 47 (2005) 175–187.
[55] A. Chandra, L.S. Turng, P. Gopalan, R.M. Rowell, S. Gong, Study of utilizing thin polymer surface coating on the nanoparticles for melt compounding of polycarbonate/alumina nanocomposites and their optical properties, Compos Sci Technol 68 (2008) 768–776.
[56] A. Chandra, L.S. Turng, K. Li, H.X. Huang, Fracture behavior and optical properties of melt compounded semi-transparent polycarbonate (PC)/alumina nanocomposites, Composites Part A 42 (2011) 1903–1909.
[57] S.B. Bae, C.K. Kim, K. Kim, I.J. Chung, The effect of organic modifiers with different chain lengths on the dispersion of clay layers in HTPB (hydroxyl terminated polybutadiene), Eur Polym J 44 (2008) 3385–3392.
[58] H. Zheng, Y. Zhang, Z. Peng, Y. Zhang, Preparation and properties of semi-transparent EPDM/montmorillonite nanocomposites, Polym Polym Compos 13 (2005) 53–60.
[59] A. Durmus, N. Ercan, G. Soyubol, A. Kasgoz, I. Aydin, Effects of compatibilizer structure on the clay dispersion and barrier properties of Polyethylene/Clay nanocomposite films, Acad J Manuf Eng 8 (2010) 49–54.
[60] A. Haase, P. Hesse, L. Brommer, O. Jacobs, C. Abetz, U.A. Handge, et al., Modification of polycarbonate and glycol modified poly(ethylene terephthalate) by addition of silica-nanoparticles grafted with SAN copolymer using “Classical” and ARGET ATRP, Macromol Mater Eng 298 (2013) 292–302.
[61] A. Chatterjee, Properties improvement of PMMA using nano TiO2, J Appl Polym Sci 118 (2010) 2890–2897.
[62] M. Farhoodi, S. Dadashi, S.M.A. Mousavi, R. Sotudeh-Gharebagh, Z. Emam-Djomeh, A.A. Oromiehie, et al., Influence of TiO 2 nanoparticle filler on the properties of PET and PLA nanocomposites, Polymer 36 (2012) 745–755.
[63] X.F. Zeng, X. Li, X. Tao, Z.G. Shen, J.F. Chen, Fabrication of highly transparent ZnO/PVB nanocomposite films with novel UV-shielding properties, Nanoelectr 3rd Int Conf, 2010777–778.
[64] C. Espejo, A. Arribas, F. Monzó, P.P. Díez, Nanocomposite films with enhanced radiometric properties for greenhouse covering applications, J Plast Film Sheeting 28 (2012) 336–350.
[65] P.J. Yoon, D.L. Hunter, D.R. Paul, Polycarbonate nanocomposites. Part 1. Effect of organoclay structure on morphology and properties, Polymer 44 (2003) 5323–5339.
[66] K.M. Lee, C.D. Han, Effect of hydrogen bonding on the rheology of polycarbonate/organoclay nanocomposites, Polymer 44 (2003) 4573–4588.
[67] J.H. Liaw, T.Y. Hsueh, T. Tan, Y. Wang, S. Chiao, Twin-screw compounding of poly (methyl methacrylate)/ clay nanocomposites : effects of compounding temperature and matrix molecular weight, Polym Int 1052 (2007) 1045–1052.
[68] D. Lerari, S. Peeterbroeck, S. Benali, A. Benaboura, P. Dubois, Use of a new natural clay to produce poly(methyl methacrylate)-based nanocomposites, Polym Int 59 (2010) 71–77.
[69] M.E. Romero-guzma, A. Romo-uribe, E. Ovalle-garcı, R. Olayo, C.A. Cruz-ramos, Microstructure and dynamic mechanical analysis of extruded layered silicate PVC nanocomposites, Polym Adv Technol 19 (2008) 1168–1176.
[70] M. Strange, D. Plackett, M. Kaasgaard, F.C. Krebs, Biodegradable polymer solar cells, Sol Energy Mater Sol Cells 92 (2008) 805–813.
[71] C. De Melo, P.S. Garcia, E.V.M. Grossmann, F. Yamashita, L.H. Dall’Antonia, S. Mali, Properties of extruded xanthan-starch-Clay nanocomposite films, Braz Arch Biol Technol 54 (2011) 1223–1233.
[72] S.I. Hong, J.W. Rhim, Preparation and properties of melt-intercalated linear low density polyethylene/clay nanocomposite films prepared by blow extrusion, LWT Food Sci Technol 48 (2012) 43–51.
[73] S. Niknezhad, A.I. Isayev, Online ultrasonic film casting of LLDPE and LLDPE/clay nanocomposites, J Appl Polym Sci 129 (2013) 263–275.
[74] F. Inceoglu, Y.Z. Menceloglu, Transparent low-density polyethylene/starch nanocomposite films, J Appl Polym Sci 129 (2013) 1907–1914.
[75] A. Singhal, G. Skandan, Engineered nanomaterial hard coatings on metal and polymer substrates, in: A. Kumar, Y.W. Chung, J.J. Moore, G.L. Doll, K. Yat-

UNCORRECTED PROOF

sui, D. Misra (Eds.), Surf Eng Sci Technol II, TMS, Pittsburgh, 2002, pp. 69–78.
[76] W.S. Wang, C.K. Liang, Y.C. Chen, Y.L. Su, T.Y. Tsai, Y.W. Chen-Yang, Transparent and flame retardant PMMA/clay nanocomposites prepared with dual modified organoclay, Polym Adv Technol 23 (2012) 625–631.
[77] S. Hsiao, G. Liou, L. Chang, Synthesis and properties of organosoluble Polyimide/Clay hybrids, J Appl Polym Sci 80 (2001) 2067–2072.
[78] O. Parlak, M.M. Demir, Anomalous transmittance of polystyrene–ceria nanocomposites at high particle loadings, J Mater Chem C 1 (2013) 290–298.
[79] S. Mallakpour, A. Barati, Efficient preparation of hybrid nanocomposite coatings based on poly(vinyl alcohol) and silane coupling agent modified TiO2 nanoparticles, Prog Org Coat 71 (2011) 391–398.
[80] S. Mallakpour, M. Dinari, Nanocomposites of poly(vinyl alcohol) reinforced with chemically modified AL2O3: synthesis and characterization, J Macromol Sci Part B 52 (2013) 1651–1661.
[81] D.W. Chae, B.C. Kim, Characterization on polystyrene/zinc oxide nanocomposites prepared from solution mixing, Polym Adv Technol 16 (2005) 846–850.
[82] W.E. van Zyl, M. García, B.A.G. Schrauwen, B.J. Kooi, J.T.M. De Hosson, H. Verweij, Hybrid Polyamide/Silica nanocomposites: synthesis and mechanical testing, Macromol Mater Eng 287 (2002) 106–110.
[83] C. Lü, Y. Cheng, Y. Liu, F. Liu, B. Yang, A facile route to ZnS–Polymer nanocomposite optical materials with high nanophase content via γ-Ray irradiation initiated bulk polymerization, Adv Mater 18 (2006) 1188–1192.
[84] H. Althues, P. Simon, F. Philipp, S. Kaskel, Integration of zinc oxide nanoparticles into transparent poly(butanediolmonoacrylate) via Photopolymerisation, J Nanosci Nanotechnol 6 (2006) 409–413.
[85] H.B. Sunkara, J.M. Jethmalani, W. Ford, Solidification of colloidal crystals of silica, ACS Symp Ser., vol. 585 (1995) 181–191, American Chemical Society.
[86] C.M. Tsai, S.H. Hsu, C.C. Ho, Y.C. Tu, H.C. Tsai, C.A. Wang, et al., High refractive index transparent nanocomposites prepared by in situ polymerization, J Mater Chem C 2 (2014) 2251–2258.
[87] H. Zhou, H. Wang, X. Tian, K. Zheng, Z. Wu, X. Ding, et al., Preparation of UV-curable transparent poly(urethane acrylate) nanocomposites with excellent UV/IR shielding properties, Compos Sci Technol 94 (2014) 105–110.
[88] Y. Luo, J. Yang, X. Dai, Y. Yang, S. Fu, Preparation and optical properties of novel transparent Al-Doped-ZnO/Epoxy nanocomposites, J Phys Chem C 113 (2009) 9406–9411.
[89] T.A. Cheema, A. Lichtner, C. Weichert, M. Böl, G. Garnweitner, Fabrication of transparent polymer-matrix nanocomposites with enhanced mechanical properties from chemically modified ZrO2 nanoparticles, J Mater Sci 47 (2012) 2665–2674.
[90] Y.Q. Li, S.Y. Fu, Y.W. Mai, Preparation and characterization of transparent ZnO/epoxy nanocomposites with high-UV shielding efficiency, Polymer 47 (2006) 2127–2132.
[91] Y.Q. Li, Y. Yang, S.Y. Fu, Photo-stabilization properties of transparent inorganic UV-filter/epoxy nanocomposites, Compos Sci Technol 67 (2007) 3465–3471.
[92] Y.Q. Li, Y. Yang, S.Y. Fu, X.Y. Yi, L.C. Wang, H.D. Chen, Transparent and light-emitting epoxy super-nanocomposites containing ZnO-QDs/SiO 2 nanocomposite particles as encapsulating materials for solid-state lighting, J Phys Chem C 112 (2008) 18616–18622.
[93] P.S. Cheng, K.M. Zeng, J.H. Chen, Preparation and characterization of transparent and UV-Shielding Epoxy/SR-494/APTMS/ZnO nanocomposites with high heat resistance and anti-static properties, J Chin Chem Soc 61 (2014) 320–328.
[94] N. Suzuki, M.B. Zakaria, Y.D. Chiang, K.C.W. Wu, Y. Yamauchi, Thermally stable polymer composites with improved transparency by using colloidal mesoporous silica nanoparticles as inorganic fillers, Phys Chem Chem Phys 14 (2012) 7427–7432.
[95] K. Jlassi, S. Chandran, M. Mičušik, M. Benna-Zayani, Y. Yagci, S. Thomas, et al., Poly(glycidyl methacrylate)-grafted clay nanofiller for highly transparent and mechanically robust epoxy composites, Eur Polym J 72 (2015) 89–101.
[96] Y. Li, P. Tao, A. Viswanath, B.C. Benicewicz, L.S. Schadler, Bimodal surface ligand engineering: the key to tunable nanocomposites, Langmuir 29 (2013) 1211–1220.
[97] V.M.F. Evora, A. Shukla, Fabrication, characterization, and dynamic behavior of polyester/TiO2 nanocomposites, Mater Sci Eng A 361 (2003) 358–366.
[98] J.L.H. Chau, Y.M. Lin, A.K. Li, W.F. Su, K.S. Chang, S.L.C. Hsu, et al., Transparent high refractive index nanocomposite thin films, Mater Lett 61 (2007) 2908–2910.
[99] C. Lü, Z. Cui, Y. Wang, Z. Li, C. Guan, B. Yang, et al., Preparation and characterization of ZnS-polymer nanocomposite films with high refractive index, J Mater Chem 13 (2003) 2189–2195.
[100] H. Zhang, Z. Cui, Y. Wang, K. Zhang, X. Ji, C. Lü, et al., From water-soluble CdTe nanocrystals to fluorescent nanocrystal–Polymer transparent composites using polymerizable surfactants, Adv Mater 15 (2003) 777–780.
[101] C.H. Hung, W.T. Whang, Effect of surface stabilization of nanoparticles on luminescent characteristics in ZnO/poly(hydroxyethyl methacrylate) nanohybrid films, J Mater Chem 15 (2005) 267–274.
[102] Y. Zhang, X. Wang, Y. Liu, S. Song, D. Liu, Highly transparent bulk PMMA/ZnO nanocomposites with bright visible luminescence and efficient UV-shielding capability, J Mater Chem 22 (2012) 11971–11977.
[103] Y. Hu, S. Zhou, L. Wu, Surface mechanical properties of transparent poly(methyl methacrylate)/zirconia nanocomposites prepared by in situ bulk polymerization, Polymer 50 (2009) 3609–3616.
[104] Y. Hu, G. Gu, S. Zhou, L. Wu, Preparation and properties of transparent PMMA/ZrO2 nanocomposites using 2-hydroxyethyl methacrylate as a coupling agentSurface mechanical properties of transparent poly(methyl methacrylate)/zirconia nanocomposites prepared by in situ bulk polymerization, Polymer 52 (2011) 122–129.
[105] E. Džunuzović, K. Jeremić, J.M. Nedeljković, In situ radical polymerization of methyl methacrylate in a solution of surface modified TiO2 and nanoparticles, Eur Polym J 43 (2007) 3719–3726.
[106] S. Li, J. Qin, A. Fornara, M. Toprak, M. Muhammed, D.K. Kim, Synthesis and magnetic properties of bulk transparent PMMA/Fe-oxide nanocomposites, Nanotechnology 20 (2009), 185607/1-6.
[107] M. Avella, M.E. Errico, E. Martuscelli, Novel PMMA/CaCO 3 nanocomposites abrasion resistant prepared by an in situ polymerization process, Nano Lett 1 (2001) 213–217.
[108] P.A. Wheeler, J. Wang, L.J. Mathias, Poly(methyl methacrylate)/Laponite nanocomposites: exploring covalent and ionic clay modifications, Chem Mater 18 (2006) 3937–3945.
[109] W. Cai, A. Wang, L. Fu, J. Hu, T. Rao, J. Wang, et al., Preparation and luminescent properties of GdOF:Ce, Tb nanoparticles and their transparent PMMA nanocomposites, Opt Mater 43 (2015) 36–41.
[110] H.T. Liu, X.F. Zeng, H. Zhao, J.F. Chen, Highly transparent and multifunctional polymer nanohybrid film with superhigh ZnO content synthesized by a bulk polymerization method, Ind Eng Chem Res 51 (2012) 6753–6759.
[111] H.R. Hakimelahi, L. Hu, B.B. Rupp, M.R. Coleman, Synthesis and characterization of transparent alumina reinforced polycarbonate nanocomposite, Polymer 51 (2010) 2494–2502.
[112] C. Guan, C. Lü, Y. Cheng, S. Song, B. Yang, A facile one-pot route to transparent polymer nanocomposites with high ZnS nanophase contents via in situ bulk polymerization, J Mater Chem 19 (2009) 617–621.
[113] S. Chen, R. Gaume, Transparent bulk size nanocomposites with high inorganic loading, Appl Phys Lett 107 (2015), 241906/1-5.
[114] H.S. Liou, B.C. Pan, G.S. Liou, Highly transparent AgNW/PDMS stretchable electrodes for elastomeric electrochromic devices, Nanoscale 9 (2017) 2633–2639.
[115] C.J. Landry, B.K. Coltrain, J.A. Wesson, N. Zumbulyadis, J.L. Lippert, In situ polymerization of tetraethoxysilane in polymers: chemical nature of the interactions, Polymer 33 (1992) 1496–1506.
[116] F. Silveira, I. Val, P. Yoshida, S.P. Nunes, Phase separation in PMMA/silica sol-gel systems, Polymer 36 (1995) 1425–1434.
[117] R. Tamaki, Y. Chujo, Synthesis of poly(vinyl alcohol)/silica gel polymer hybrids by in-situ hydrolysis method, Appl Organomet Chem 12 (1998) 755–762.
[118] K. Nakane, T. Yamashita, K. Iwakura, F. Suzuki, Properties and structure of poly(vinyl alcohol)/silica composites, J Appl Polym Sci 74 (1999) 133–138.
[119] C.J.T. Landry, B.K. Coltrain, M.R. Landry, J.J. Fitzgerald, V.K. Long, Poly (viny1 acetate)/ silica filled materials : material properties of in situ vs fumed silica particles, Macromolecules 26 (1993) 3702–3712.
[120] Y. Chujo, T. Saegusa, Organic polymer hybrids with silica gel formed by means of the sol-gel method, Macromol Synth Order Adv Prop 100 (1992) 11–29.
[121] Y. Chujo, Organic–Inorganic nano-hybrid materials, Kona Powder Part J 25 (2007) 255–260.
[122] R. Sengupta, A. Bandyopadhyay, S. Sabharwal, T.K. Chaki, A.K. Bhowmick, Polyamide-6,6/in situ silica hybrid nanocomposites by sol–gel technique: synthesis, characterization and properties, Polymer 46 (2005) 3343–3354.
[123] M.W. Ellsworth, B.M. Novak, Mutually interpenetrating Inorganic-Organic networks. New routes into nonshrinking sol-gel composite materials, J Am Chem Soc 113 (1991) 2756–2758.
[124] R. Tamaki, Y. Chujo, Synthesis of chitosan/silica gel polymer hybrids, Compos Interfaces 6 (1998) 259–272.
[125] L. Bokobza, A.L. Diop, Reinforcement of poly(dimethylsiloxane) by sol-gel in situ generated silica and titania particles, Express Polym Lett 4 (2010) 355–363.
[126] N. Juangvanich, K.A. Mauritz, Polyethersulfone – [silicon oxide] hybrid materials via in Situ Sol – gel reactions for tetra-alkoxysilanes, J Appl Polym Sci 67 (1998) 1799–1810.
[127] B.K. Coltrain, W.T. Ferrar, C.J.T. Landry, T.R. Molaire, N. Zumbulyadis, Polyphosphazene molecular composites. 1. In situ polymerization of tetraethoxysilane, Chem Mater 4 (1992) 358–364.

UNCORRECTED PROOF

[128] W.T. Ferrar, B.K. Coltrain, C.J.T. Landry, V.K. Long, T.R. Molaire, D.E. Schildkraut, Polyphosphazene molecular composites. In situ polymerizations of silicon, titanium, zirconium, and aluminum alkoxides, in: P. Wisian-Neilson, H.R. Allcock, K. Wynne (Eds.), Inorganic and organometalic polymers II, American Chemical Society, Washington, DC, 1994, pp. 258–267.
[129] R. Tamaki, Y. Chujo, Synthesis of polystyrene and silica gel polymer hybrids utilizing ionic interactions, Chem Mater 11 (1999) 1719–1726.
[130] R. Tamaki, K. Samura, Y. Chujo, Synthesis of polystyrene and silica gel polymer hybrids via π–π interactions, Chem Commun (1998) 1131–1132.
[131] G.H. Hsiue, J.K. Chen, Y.L. Liu, Synthesis and characterization of nanocomposite of polyimide – silica hybrid from nonaqueous sol – gel process, J Appl Polym Sci 76 (2000) 1609–1618.
[132] S.P. Nunes, K.V. Peinemann, K. Ohlrogge, A. Alpers, M. Keller, A.T.N. Pires, Membranes of poly(ether imide) and nanodispersed silica, J Membr Sci 157 (1999) 219–226.
[133] Y. Wei, W. Wang, J.M. Yeh, B. Wang, D. Yang, J.K. Murray Jr, et al., Vinyl-polymer-Modified hybrid materials and photoacid-catalyzed sol—gel reactions, ACS Symp Ser 565 (1995) 125–141.
[134] Y. Wei, D. Yang, L. Tang, M.K. Hutchins, Synthesis, characterization, and properties of new polystyrene-SiO2 hybrid sol-gel materials, J Mater Res 8 (1993) 1143–1152.
[135] H. Wang, P. Xu, W. Zhong, L. Shen, Q. Du, Transparent poly(methyl methacrylate)/silica/zirconia nanocomposites with excellent thermal stabilities, Polym Degrad Stab 87 (2005) 319–327.
[136] G.H. Hsiue, W.J. Kuo, Y.P. Huang, R.J. Jeng, Microstructural and morphological characteristics of PS – SiO 2 nanocomposites, Polymer 41 (2000) 2813–2825.
[137] Q. Hu, E. Marand, In situ formation of nanosized TiO 2 domains within poly (amide – imide) by a sol – gel process, Polymer 40 (1999) 4833–4843.
[138] S.X. Wang, M.T. Wang, Y. Lei, L. Zhang, "Anchor effect" in poly(styrene maleic anhydride)/TiO2 nanocomposites, J Mater Sci Lett 18 (1999) 2009–2012.
[139] F. Suzuki, K. Onozato, Y. Kurokawa, A formation of compatible poly(vinyl alcohol)/alumina gel composite and its properties, J Appl Polym Sci 39 (1990) 371–381.
[140] T. Du, H. Song, O.J. Ilegbusi, Sol-gel derived ZnO/PVP nanocomposite thin film for superoxide radical sensor, Mater Sci Eng C 27 (2007) 414–420.
[141] R.F. Ziolo, E.P. Giannelis, B.A. Weinstein, M.P. O'horo, B.N. Ganguly, V. Mehrotra, et al., Matrix-mediated synthesis of nanocrystalline ggr-Fe2O3: a new optically transparent magnetic material, Science 257 (1992) 219–223.
[142] S. Porel, N. Venkatram, D.N. Rao, T.P. Radhakrishnan, In situ synthesis of metal nanoparticles in polymer matrix and their optical limiting applications, J Nanosci Nanotechnol 7 (2007) 1887–1892.
[143] D.C. Onwudiwe, T.P.J. Krüger, O.S. Oluwatobi, C.A. Strydom, Nanosecond laser irradiation synthesis of CdS nanoparticles in a PVA system, Appl Surf Sci 290 (2014) 18–26.
[144] D.J. Asunskis, I.L. Bolotin, L. Hanley, Nonlinear optical properties of PbS nanocrystals grown in polymer solutions, J Phys Chem C 112 (2008) 9555–9558.
[145] A.M. Sajimol, P.B. Anand, K.M. Anilkumar, S. Jayalekshmi, Exceptionally good, transparent and flexible FeS 2 /poly(vinyl pyrrolidone) and FeS 2 /poly(vinyl alcohol) nanocomposite thin films with excellent UV-shielding properties, Polym Int 62 (2013) 670–675.
[146] T. Kyprianidou-leodidou, P. Margraf, W. Caseri, U.W. Suter, P. Walther, Polymer sheets with a thin nanocomposite layer acting as a UV filter, Polym Adv Technol 8 (1997) 505–512.
[147] H. Du, G.Q. Xu, W.S. Chin, L. Huang, Ji W. Synthesis, Characterization, and nonlinear optical properties of hybridized CdS−Polystyrene nanocomposites, Chem Mater 14 (2002) 4473–4479.
[148] P. Hajji, L. David, J.F. Gerard, H. Kaddami, J.P. Pascault, G. Vigier, Synthesis-morphology-Mechanical properties relationships of polymer-silica nanocomposite hybrid materials, MRS Online Proc Libr 576 (1999) 357–362.
[149] P. Hajji, L. David, J.F. Gerard, J.P. Pascault, G. Vigier, Synthesis, Structure, and Morphology of Polymer – Silica Hybrid Nanocomposites Based on Hydroxyethyl Methacrylate, J Polym Sci Part B: Polym Phys 37 (1999) 3172–3187.
[150] B.M. Novak, C. Davies, "Inverse" Organic-Inorganic Composite Materials. 2. Free-Radical Routes into nonshriking sol-gel composites, Macomolecules 24 (1991) 5481–5483.
[151] S. Wang, Z. Ahmad, J.E. Mark, A polyamide-silica composite prepared by the sol-gel process, Polym Bull 31 (1993) 323–330.
[152] L. Matgj, K. Dusek, J. Plegtil, J. Kg, F. Ledni cklj, Formation and structure of the epoxy-silica aybrids, Polymer 40 (1998) 171–181.
[153] C.V. Avadhani, Y. Chujo, Polyimide – silica gel hybrids containing metal salts : preparation via the sol – gel reaction, Appl Organomet Chem 11 (1997) 153–161.
[154] Y. Wei, W. Wang, J.M. Yeh, B. Wang, D. Yang, J.K. Murray, Photochemical synthesis of polyacrylate–silica hybrid sol–gel materials catalyzed by photoacids, Adv Mater 6 (1994) 372–374.
[155] A.H. Yuwono, Y. Zhang, J. Wang, Investigating the nanostructural evolution of TiO2 nanoparticles in the sol-gel derived TiO2-polymethyl methacrylate nanocomposites, Int J Technol 1 (2010) 11–19.
[156] R. Palkovits, H. Althues, A. Rumplecker, B. Tesche, A. Dreier, U. Holle, et al., Polymerization of w/o microemulsions for the preparation of transparent SiO2 /PMMA nanocomposites, Langmuir 21 (2005) 6048–6053.
[157] F.M. Pavel, R.A. Mackay, Reverse micellar synthesis of a Nanoparticle/Polymer composite, Langmuir 16 (2000) 8568–8574.
[158] Y. Nakao, Preparation and Characterisation of Noble Metal Solid Sols in poly (methy1 methacrylate), J Chem Soc Chem Commun (1993) 826–828.
[159] L. Balan, D. Burget, Synthesis of metal/polymer nanocomposite by UV-radiation curing, Eur Polym J 42 (2006) 3180–3189.
[160] A. Akhavan, N. Sheikh, R. Beteshobabrud, Polymethylmethacrylate/Silver nanocomposite prepared by γ-Ray, J Nucl Sci Tech 50 (2010) 80–84.
[161] L. Zhang, F. Li, Y. Chen, X. Wang, Synthesis of transparent ZnO/PMMA nanocomposite films through free-radical copolymerization of asymmetric zinc methacrylate acetate and in-situ thermal decomposition, J Lumin 131 (2011) 1701–1706.
[162] A. İncel, T. Güner, O. Parlak, M.M. Demir, Null extinction of Ceria@silica hybrid particles: transparent polystyrene composites, ACS Appl Mater Interfaces 7 (2015) 27539–27546.
[163] C.W. Hsu, B. Zhen, W. Qiu, O. Shapira, B.G. DeLacy, J.D. Joannopoulos, et al., Transparent displays enabled by resonant nanoparticle scattering, Nat Commun 5 (2014) 3152–3158.
[164] S. Ehlert, C. Stegelmeier, D. Pirner, S. Förster, A general route to optically transparent highly filled polymer nanocompositesle, Macromolecules 48 (2015) 5323–5327.
[165] P. Tao, A. Viswanath, Y. Li, R.W. Siegel, B.C. Benicewicz, L.S. Schadler, Bulk transparent epoxy nanocomposites filled with poly(glycidyl methacrylate) brush-grafted TiO2 nanoparticles, Polymer 54 (2013) 1639–1646.
[166] P.G. De Gennes, Conformations of polymers attached to an interface, Macromolecules 13 (1980) 1069–1075.
[167] A.S. Robbes, F. Cousin, F. Meneau, F. Dalmas, R. Schweins, D. Gigmes, et al., Polymer-grafted magnetic nanoparticles in nanocomposites: curvature effects, conformation of grafted chain, and bimodal nanotriggering of filler organization by combination of chain grafting and magnetic field, Macromolecules 45 (2012) 9220–9231.
[168] D. Sunday, J. Ilavsky, D.L. Green, A phase diagram for polymer-grafted nanoparticles in homopolymer matrices, Macromolecules 45 (2012) 4007–4011.
[169] C. Chevigny, F. Dalmas, E. Di Cola, D. Gigmes, D. Bertin, F. Boué, et al., Polymer-grafted-nanoparticles nanocomposites: dispersion, grafted chain conformation, and rheological behavior, Macromolecules 44 (2011) 122–133.
[170] B. Natarajan, T. Neely, A. Rungta, B.C. Benicewicz, L.S. Schadler, Thermomechanical properties of bimodal brush modified nanoparticle composites, Macromolecules 46 (2013) 4909–4918.
[171] A. Rungta, B. Natarajan, T. Neely, D. Dukes, L.S. Schadler, B.C. Benicewicz, Grafting bimodal polymer brushes on nanoparticles using controlled radical polymerization, Macromolecules 45 (2012) 9303–9311.
[172] M. Annaka, K. Mortensen, T. Matsuura, M. Ito, K. Nochioka, N. Ogata, Organic–inorganic nanocomposite gels as an in situ gelation biomaterial for injectable accommodative intraocular lens, Soft Matter 8 (2012) 7185–7196.
[173] J.H. Li, R.Y. Hong, M.Y. Li, H.Z. Li, Y. Zheng, J. Ding, Effects of ZnO nanoparticles on the mechanical and antibacterial properties of polyurethane coatings, Prog Org Coat 64 (2009) 504–509.
[174] M.I. Sarwar, S. Zulfiqar, Z. Ahmad, Polyamide – silica nanocomposites : mechanical, morphological and thermomechanical investigations, Polym Int 57 (2008) 292–296.
[175] L. Billon, M. Save, M Cunningham, Surface-initiated nitroxide mediated polymerization, in: D. Gigmes (Ed.), Nitroxide mediat. Polym from fundamentals to applications in materials science, Royal Society of Chemistry, Cambridge, 2016, pp. 406–440.
[176] Z.W. Liu, C.N. Chuang, W.Y. Chang, Y.W. Pa, S.C. Wang, S.H. Chen, et al., Multi-functional urethane epoxy acrylates (UEAs) and their visible-light cured UEA/MSMA-colloid silica nanocomposite films as reinforcement on polycarbonate matrix, Colloids Surf A 514 (2017) 178–184.
[177] J.M. Kubiak, J. Yan, J. Pietrasik, K. Matyjaszewski, Toughening PMMA with fillers containing polymer brushes synthesized via atom transfer radical polymerization (ATRP), Polymer 117 (2017) 48–53.
[178] R. Matsuno, H. Otsuka, A. Takahara, Polystyrene-grafted titanium oxide nanoparticles prepared through surface-initiated nitroxide-mediated radical polymerization and their application to polymer hybrid thin films, Soft Matter 2 (2006) 415–421.

UNCORRECTED PROOF

[179] V. Melinte, A. Chibac, T. Buruiana, E.C. Buruiana, Hybrid nanocomposites prepared by in situ photopolymerization using photoinitiator-modified montmorillonite, Prog Org Coat 104 (2017) 125–134.
[180] D. Maillard, S.K. Kumar, B. Fragneaud, J.W. Kysar, A. Rungta, B.C. Benicewicz, et al., Mechanical properties of thin glassy polymer films filled with spherical polymer-grafted nanoparticles, Nano Lett 12 (2012) 3909–3914.
[181] S. Sun, Z. Pan, F.K. Yang, Y. Huang, B. Zhao, A transparent silica colloidal crystal/PDMS composite and its application for crack suppression of metallic coatings, J Colloid Interface Sci 461 (2016) 136–143.
[182] X. Yin, Y. Feng, Q. Zhao, Y. Li, S. Li, H. Dong, et al., Highly transparent, strong, and flexible fluorographene/fluorinated polyimide nanocomposite films with low dielectric constant, J Mater Chem C 6 (2018) 6378–6384.
[183] S. Kim, C.A. Wilkie, Transparent and flame retardant PMMA nanocomposites, Polym Adv Technol 19 (2008) 496–506.
[184] P.K. Khanna, N. Singh, Light emitting CdS quantum dots in PMMA: synthesis and optical studies, J Lumin 127 (2007) 474–482.
[185] M.M. Demir, M. Memesa, P. Castignolles, G. Wegner, PMMA/zinc oxide nanocomposites prepared by in-situ bulk polymerization, Macromol Rapid Commun 27 (2006) 763–770.
[186] M. Wang, X.W. Han, L. Liu, X.F. Zeng, H.K. Zou, J.X. Wang, et al., Transparent aqueous Mg(OH) 2 nanodispersion for transparent and flexible polymer film with enhanced flame-retardant property, Ind Eng Chem Res 54 (2015) 12805–12812.
[187] Y. Cheng, Z. Lin, H. Lü, L. Zhang, B. Yang, ZnS nanoparticles well dispersed in ethylene glycol: coordination control synthesis and application as nanocomposite optical coatings, Nanotechnology 25 (2014), 115601/1-9.
[188] A. Romo-Uribe, J.A. Arcos-Casarrubias, A. Reyes-Mayer, R. Guardian-Tapia, Acrylate hybrid nanocomposite coatings based on SiO2 nanoparticles. In-situ semi-batch emulsion polymerization, Eur Polym J 76 (2016) 170–187.
[189] M.A. Mumin, K.F. Akhter, S. Dresser, S.T. Van Dinther, W. Wu, P.A. Charpentier, Multifunctional mesoporous silica nanoparticles in poly(ethylene-co-vinyl acetate) for transparent heat retention films, J Polym Sci Part B: Polym Phys 53 (2015) 851–859.
[190] M.A. Priolo, D. Gamboa, J.C. Grunlan, Transparent clay-polymer nano brick wall assemblies with tailorable oxygen barrier, ACS Appl Mater Interfaces 2 (2010) 312–320.
[191] A.M. Youssef, A.M. El-Nahrawy, A.B.A. Hammad, Sol-gel synthesis and characterizations of hybrid chitosan-PEG/calcium silicate nanocomposite modified with ZnO-NPs and (E102) for optical and antibacterial applications, Int J Biol Macromol 97 (2017) 561–567.
[192] W.N. Nkeuwa, B. Riedl, V. Landry, UV-cured clay/based nanocompoqite topcoats for wood furniture: part I: morphological study, water vapor transmission rate and optical clarity, Prog Org Coat 77 (2014) 1–11.
[193] D.J. Kang, G.U. Park, H.Y. Park, H.G. Im, A robust transparent encapsulation material: silica nanoparticle-embedded epoxy hybrid nanocomposite, Compos Sci Technol 144 (2017) 107–113.
[194] M. Wong, R. Ishige, K.L. White, P. Li, D. Kim, R. Krishnamoorti, et al., Large-scale self-assembled zirconium phosphate smectic layers via a simple spray-coating process, Nat Commun 5 (2014) 3589–3601.
[195] H. Kim, H. Ra, H. Kim, H.G. Kim, S.S. Kim, Enhancement of barrier properties by wet coating of epoxy-ZrP nanocomposites on various inorganic layers, Prog Org Coat 108 (2017) 25–29.
[196] P. Das, J.M. Malho, K. Rahimi, F.H. Schacher, B. Wang, D.E. Demco, et al., Nacre-mimetics with synthetic nanoclays up to ultrahigh aspect ratios, Nat Commun 6 (2015) 5967–5981.
[197] W. Lee, S.C. Gil, H. Kim, K. Han, H. Lee, Partially sulfonated Poly(arylene ether sulfone)/organically modified metal oxide nanoparticle composite membranes for proton exchange membrane for direct methanol fuel cell, Compos Sci Technol 129 (2016) 101–107.
[198] J. Bae, J. Lee, C.S. Park, O.S. Kwon, C.S. Lee, Fabrication of photo-crosslinkable polymer/silica sol–gel hybrid thin films as versatile barrier films, J Ind Eng Chem 38 (2016) 61–66.
[199] J. Hu, M. Chen, L. Wu, Organic-inorganic nanocomposites synthesized via miniemulsion polymerization, Polym Chem 2 (2011) 760–772.
[200] C.W. Hsu, C.C.M. Ma, C.S. Tan, H.T. Li, W.B. Chen, S.C. Huang, Synthesis of a liquid zirconium hybrid resin and the ability of the resin to accelerate the curing of a transparent silicone-modified cycloaliphatic epoxy nanocomposite, Polym Int 64 (2015) 1268–1274.
[201] T. Hosoya, W. Sakamoto, T. Yogo, Transparent and self-standing manganese zinc ferrite nanoparticle/cellulose hybrid films, Mater Lett 137 (2014) 491–494.
[202] W. Caseri, Nanocomposites of polymers and metals or semiconductors : historical background and optical properties, Macromol Rapid Commun 21 (2000) 705–722.
[203] L. Truffault, Synthèse et caractérisation de nanoparticules à base d'oxydes de cérium et de fer pour la filtration des UV dans les produits solaires. PhD Thesis, Université d'Orléans, Orléans Fr, 2010, 192 pp.
[204] V. Khrenov, M. Klapper, M. Koch, K. Müllen, Surface functionalized ZnO particles designed for the use in transparent nanocomposites, Macromol Chem Phys 206 (2005) 95–101.
[205] S. Hess, M.M. Demir, V. Yakutkin, S. Baluschev, G. Wegner, Investigation of oxygen permeation through composites of PMMA and surface-modified ZnO nanoparticles, Macromol Rapid Commun 30 (2009) 394–401.
[206] M.S. Augustine, P.P. Jeeju, V.G. Sreevalsa, S. Jayalekshmi, Excellent UV absorption in spin-coated thin films of oleic acid modified zinc oxide nanorods embedded in Polyvinyl alcohol, J Phys Chem Solids 73 (2012) 396–401.
[207] A. Ammala, A.J. Hill, P. Meakin, S.J. Pas, T.W. Turney, Degradation studies of polyolefins incorporating transparent nanoparticulate zinc oxide UV stabilizers, J Nanopart Res 4 (2002) 167–174.
[208] R.J. Nussbaumer, W.R. Caseri, P. Smith, T. Tervoort, Polymer-TiO2 nanocomposites: a route towards visually transparent broadband UV filters and high refractive index materials, Macromol Mater Eng 288 (2003) 44–49.
[209] R.J. Nussbaumer, W. Caseri, T. Tervoort, P. Smith, Synthesis and characterization of surface-modified rutile nanoparticles and transparent polymer composites thereof, J Nanopart Res 4 (2002) 319–323.
[210] L. Cano, E. Pollet, L. Avérous, A. Tercjak, Effect of TiO2 nanoparticles on the properties of thermoplastic chitosan-based nano-biocomposites obtained by mechanical kneading, Composites Part A 93 (2017) 33–40.
[211] T. Masui, M. Yamamoto, T. Sakata, H. Mori, G. Adachi, Synthesis of BN-coated CeO2 fine powder as a new UV blocking material, J Mater Chem 10 (2000) 353–357.
[212] D. Sun, N. Miyatake, H.J. Sue, Transparent PMMA/ZnO nanocomposite films based on colloidal ZnO quantum dots, Nanotechnology 18 (2007), 215606/1-6.
[213] J. Godnjavec, B. Znoj, J. Vince, M. Steinbucher, A. Žnidaršič, P. Venturini, Stabilization of rutile tio 2 nanoparticles with glymo in polyacrylic clear coating, Mater Tehnol 46 (2012) 19–24.
[214] S. Li, M.S. Toprak, Y.S. Jo, J. Dobson, D.K. Kim, M. Muhammed, Bulk synthesis of transparent and homogeneous polymeric hybrid materials with ZnO quantum dots and PMMA, Adv Mater 19 (2007) 4347–4352.
[215] M. Xiong, G. Gu, B. You, L. Wu, Preparation and Characterization of Poly (styrene butylacrylate) Latex/Nano-ZnO Nanocomposites, J Appl Polym Sci 90 (2003) 1923–1931.
[216] P.P. Jeeju, A.M. Sajimol, V.G. Sreevalsa, S.J. Varma, S. Jayalekshmi, Size-dependent optical properties of transparent, spin-coated polystyrene/ZnO nanocomposite films, Polym Int 60 (2011) 1263–1268.
[217] M. Khan, M. Chen, C. Wei, J. Tao, N. Huang, Z. Qi, et al., Synthesis at the nanoscale of ZnO into poly(methyl methacrylate) and its characterization, Appl Phys A 117 (2014) 1085–1093.
[218] S. Soumya, A.P. Mohamed, L. Paul, K. Mohan, S. Ananthakumar, Near IR reflectance characteristics of PMMA/ZnO nanocomposites for solar thermal control interface films, Sol Energy Mater Sol Cells 125 (2014) 102–112.
[219] S. Moussa, F. Namouchi, H. Guermazi, Fabrication, structural and optical investigations of ZnO/epoxy nanocompositestle, Eur Phys J Plus 130 (2015) 152–161.
[220] X. Zhao, L. Li, Y. Liu, C.P. Wong, UVA-shielding silicone/zinc oxide nanocomposite coating for automobile windows, Polym Compos 37 (2015) 2053–2057.
[221] S. Zhang, J. Li, X. Guo, L. Liu, H. Wei, Y. Zhang, Nanostructured composite films of ceria nanoparticles with anti-UV and scratch protection properties constructed using a layer-by-layer strategy, Appl Surf Sci 382 (2016) 316–322.
[222] P. Tao, A. Viswanath, L.S. Schadler, B.C. Benicewicz, R.W. Siegel, Preparation and optical properties of indium tin oxide/epoxy nanocomposites with polyglycidyl methacrylate grafted nanoparticles, ACS Appl Mater Interfaces 3 (2011) 3638–3645.
[223] G.J. Zhang, Z.H. Chen, X.R. Zeng, F. Yu, J. Wang, Preparation and characterization of poly(MMA-BA)/nano-ATO hybrid latex via miniemulsion polymerization, J Coat Technol Res 8 (2011) 505–511.
[224] H. Liu, X. Zeng, X. Kong, S. Bian, J. Chen, A simple two-step method to fabricate highly transparent ITO/polymer nanocomposite films, Appl Surf Sci 258 (2012) 8564–8569.
[225] T. Druffel, N. Mandzy, M. Sunkara, E. Grulke, Polymer nanocomposite thin film mirror for the infrared region, Small 4 (2008) 459–461.
[226] N.G. Ireni, M. Karuppaiah, R. Narayan, Raju KVSN, P. Basak, TiO2/ Poly(thiourethane-urethane)-urea nanocomposites: anticorrosion materials with NIR-reflectivity and high refractive index, Polymer 119 (2017) 142–151.
[227] W. Heffels, J. Friedrich, C. Darribère, J. Teisen, K. Interewicz, C. Bastiaansen, et al., Polymers and metals: nanocomposites and complex salts with metallic chain structure, Recent Res Dev Macromol Res 2 (1999) 143–156.
[228] G. Carotenuto, Synthesis and characterization of poly(N-vinylpyrrolidone) filled by monodispersed silver clusters with controlled size, Appl Organomet Chem 15 (2001) 344–351.
[229] G. Carotenuto, L. Nicolais, Synthesis and characterization of gold-based nanoscopic additives for polymers, Compos Part B Eng 35 (2004) 385–391.

UNCORRECTED PROOF

[230] A. Biswas, O.C. Aktas, J. Kanzow, U. Saeed, T. Strunskus, V. Zaporojtchenko, et al., Polymer–metal optical nanocomposites with tunable particle plasmon resonance prepared by vapor phase co-deposition, Mater Lett 58 (2004) 1530–1534.
[231] F. Kirchner, R. Zsigmondy, The causes of the color changes of gold-gelatine compounds, Ann Phys 15 (1904) 573–595.
[232] L. Liu, M. Yu, J. Zhang, B. Wang, W. Liu, Y. Tang, Facile fabrication of color-tunable and white light emitting nano-composite films based on layered rare-earth hydroxides, J Mater Chem C 3 (2015) 2326–2333.
[233] T. Kyprianidou-leodidou, W. Caseri, U.W. Suter, Size variation of PbS particles in high-refractive-Index nanocomposites, J Phys Chem 98 (1994) 8992–8997.
[234] C. Lü, C. Guan, Y. Liu, Y. Cheng, B. Yang, PbS/polymer nanocomposite optical materials with high refractive index, Chem Mater 17 (2005) 2448–2454.
[235] J.L.H. Chau, C.T. Tung, Y.M. Lin, A.K. Li, Preparation and optical properties of titania/epoxy nanocomposite coatings, Mater Lett 62 (2008) 3416–3418.
[236] N. Nakayama, T. Hayashi, Preparation and characterization of TiO 2 and polymer nanocomposite films with high refractive index, J Appl Polym Sci 105 (2007) 3662–3672.
[237] C.M. Chang, C.L. Chang, C.C. Chang, Synthesis and optical properties of soluble Polyimide/Titania hybrid thin films, Macromol Mater Eng 291 (2006) 1521–1528.
[238] T.T. Huang, C.L. Tsai, S. Tateyama, T. Kaneko, G.S. Liou, Highly transparent and flexible bio-based polyimide/TiO2 and ZrO2 hybrid films with tunable refractive index, Abbe number, and memory properties, Nanoscale 8 (2016) 12793–12802.
[239] T. Asai, W. Sakamoto, T. Yogo, In situ synthesis of transparent TiO2 nanoparticle/polymer hybrid, J Mater Sci 48 (2013) 7503–7509.
[240] T. Tsuzuki, Abnormal transmittance of refractive-index-Modified ZnO/Organic hybrid films, Macromol Mater Eng 293 (2008) 109–113.
[241] C.L. Tsai, G.S. Liou, Highly transparent and flexible polyimide/ZrO 2 nanocomposite optical films with a tunable refractive index and Abbe number, Chem Commun 51 (2015) 13523–13526.
[242] T.T. Huang, S.W. Cheng, C.L. Tsai, G.S. Liou, Optically isotropic, colorless, and flexible PITEs/TiO 2 and ZrO 2 hybrid films with tunable refractive index, abbe number, and memory properties, Sci Rep 7 (2017), 7978/1-10.
[243] L. Zimmermann, M. Weibel, W. Caseri, U.W. Suter, High refractive index films of polymer nanocomposites, J Mater Res 8 (1993) 1742–1748.
[244] L. Zimmermann, M. Weibel, W. Caseri, U.W. Suter, P. Walther, Polymer nanocomposites with “Ultralow” refractive index, Polym Adv Technol 4 (1993) 1–7.
[245] I. Bodurov, T. Yovcheva, S. Sainov, PMMA films refractive index modulation via TiO2 nanoparticle inclusions and corona poling, Colloid Polym Sci 292 (2014) 3045–3048.
[246] Y. Shen, L. Wang, H. Zhang, T. Wu, H. Pan, Preparation and characterization of titania/silicone nanocomposite material, IOP Conf Ser Mater Sci Eng 87 (2015), 012021/1-5.
[247] Q. Zhang, K. Su, M.B. Chan-Park, H. Wu, D. Wang, R. Xu, Development of high refractive ZnS/PVP/PDMAA hydrogel nanocomposites for artificial cornea implants, Acta Biomater 10 (2014) 1167–1176.
[248] N. Nakayama, T. Hayashi, Preparation and characterization of TiO2–ZrO2 and thiol-acrylate resin nanocomposites with high refractive index via UV-induced crosslinking polymerization, Composites Part A 38 (2007) 1996–2004.
[249] Z.K. Heiba, M.B. Mohamed, N.G. Imam, Fine-tune optical absorption and light emitting behavior of the CdS/PVA hybridized film nanocomposite, J Mol Struct 1136 (2017) 321–329.
[250] H. Althues, R. Palkovits, A. Rumplecker, P. Simon, W. Sigle, M. Bredol, et al., Synthesis and characterization of transparent luminescent ZnS : Mn/PMMA nanocomposites, Chem Mater 18 (2006) 1068–1072.
[251] D. Sun, H.J. Sue, Tunable ultraviolet emission of ZnO quantum dots in transparent poly(methyl methacrylate), Appl Phys Lett 94 (2009), 253106/1-3.
[252] Fu Y.S. Du XW, J. Sun, X. Han, J. Liu, Complete UV emission of ZnO nanoparticles in a PMMA matrix, Semicond Sci Technol 21 (2006) 1202–1206.
[253] A.M. Alam, Z.K. Ghouri, N.A.M. Barakat, P.S. Saud, M. Park, H.Y. Kim, Photoluminescent and transparent Nylon-6 nanofiber mat composited by CdSe@ZnS quantum dots and poly (methyl methacrylate), Polymer 85 (2016) 89–95.
[254] P. Tao, Y. Li, R.W. Siegel, L.S. Schadler, Transparent luminescent silicone nanocomposites filled with bimodal PDMS-brush-grafted CdSe quantum dots, J Mater Chem C 1 (2013) 86–94.
[255] Y. Sasaki, S. Takeshita, T. Isobe, Preparation, photoluminescence, and photostability of transparent composite films of glycothermally synthesized YAG:Ce 3+ nanoparticles for white LED, ECS J Solid State Sci Technol 5 (2016) R3049–54.
[256] M. Taghavi, M. Ghaemy, S.M.A. Nasab, M. Hassanzadeh, Polyamidation of a diamine-phenol compound in ionic liquid: preparation and properties of polyamides/epoxide-functionalized γ-Al2O3 composites, J Polym Res 22 (2015) 1–12.
[257] K. Matsuyama, Y. Maeda, T. Matsuda, T. Okuyama, H. Muto, Formation of poly(methyl methacrylate)-ZnO nanoparticle quantum dot composites by dispersion polymerization in supercritical CO2, J Supercrit Fluids 103 (2015) 83–89.
[258] D. Schmid, U.A. Handge, J.P. Gann, M. Yan, W. Caseri, Melt elongation of polymer nanocomposites: a method for the controlled production of dichroic films, Macromol Mater Eng 293 (2008) 471–478.
[259] C.J. Murphy, C.J. Orendorff, Alignment of gold nanorods in polymer composites and on polymer surfaces, Adv Mater 17 (2005) 2173–2177.
[260] J. Pérez-Juste, B. Rodríguez-González, P. Mulvaney, L.M. Liz-Marzán, Optical control and patterning of gold-nanorod-Poly(vinyl alcohol) nanocomposite films, Adv Funct Mater 15 (2005) 1065–1071.
[261] B. Kulyk, B. Sahraoui, O. Krupka, V. Kapustianyk, V. Rudyk, E. Berdowska, et al., Linear and nonlinear optical properties of ZnO/PMMA nanocomposite films, J Appl Phys 106 (2009), 093102/1-6.
[262] H.I. Elim, W. Ji, A.H. Yuwono, J.M. Xue, J. Wang, Ultrafast optical nonlinearity in poly(methylmethacrylate)-TiO2 nanocomposites, Appl Phys Lett 82 (2003) 2691–2693.
[263] A.H. Yuwono, B. Liu, J. Xue, J. Wang, H.I. Elim, W. Ji, et al., Controlling the crystallinity and nonlinear optical properties of transparent TiO 2 – PMMA nanohybrids, J Mater Chem 14 (2004) 2978–2987.
[264] A.H. Yuwono, J. Xue, J. Wang, H.I. Elim, W. Ji, Titania-PMMA nanohybrids of enhanced nanocrystallinity, J Electroceram 16 (2006) 431–439.

UNCORRECTED PROOF